

Investigation of Fiber Reinforced Cementitious Matrix Composite Wrapped Stack bonded Brick Masonry under Compressive Load

GALI SAHITH

A Dissertation Submitted to
Indian Institute of Technology Hyderabad
In Partial Fulfillment of the Requirements for
The Degree of Master of Technology



भारतीय प्रौद्योगिकी संस्थान हैदराबाद
Indian Institute of Technology Hyderabad

Department of Civil Engineering

July, 2012

Declaration

I declare that this written submission represents my ideas in my own words, and where others' ideas or words have been included, I have adequately cited and referenced the original sources. I also declare that I have adhered to all principles of academic honesty and integrity and have not misrepresented or fabricated or falsified any idea/data/fact/source in my submission. I understand that any violation of the above will be a cause for disciplinary action by the Institute and can also evoke penal action from the sources that have thus not been properly cited, or from whom proper permission has not been taken when needed.

G. Sahithy

(Signature)

Gali Sahith

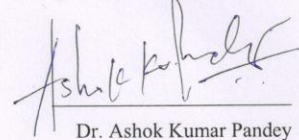
(- Student Name -)

CE10M02

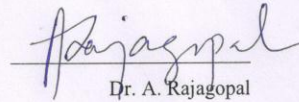
(Roll No)

Approval Sheet

This thesis entitled **“Investigation of Fiber Reinforced Cementitious Matrix composite wrapped stack bonded brick masonry under compressive loads”** by Gali Sahith is approved for the degree of Master of Technology from IIT Hyderabad.

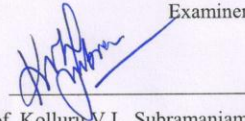


Dr. Ashok Kumar Pandey
Examiner and Chairman



Dr. A. Rajagopal

Examiner



Prof. Kolluru V.L. Subramaniam
Adviser

Acknowledgements

First of all, I would like to express my deep gratitude to my thesis adviser Kolluru. V. L. Subramaniam, Professor, Department of Civil Engineering. I am greatly indebted to him for his unwavering commitment, thought provoking and constructive comments to improve my work. He has always been a source of encouragement and has helped me tide over many a bad patch in my research work. I am bound to thank him for encouraging, working and spending precious time with me in all my tough times patiently. I learnt many more things other than research, even more about life and it had strong impact on my life for being a better person.

I would like to thank M. Ramji, Assistant Professor, Department of Mechanical Engineering, for helping out to carry correlations for my work in Engineering Optics Lab.

It has been wonderful journey. I thank all my faculty who has been exceptional in their fields taught me and also for the way they have been friendly and easily approachable. Special thanks to my classmates for making my life still easier in the stay.

Finally, I would like to thank all my family, for their love, support and constant encouragement.

ABSTRACT

Masonry construction is the most ancient construction practice that is still in use in the modern era. Some of the existing masonry structures have survived for several hundreds of years. Most of the existing masonry structures were built using available knowledge or as per the available codes of practice. With passage of time these masonry structures are in need of restoration and strengthening as many of the structures have become part of cultural heritage with a high social value

Brick masonry is composite material composed of two materials with different properties: stiffer clay bricks and relatively softer mortar. In structural applications, brick masonry is used primarily as a compression carrying member. Under compression, the resulting shear stresses at the brick-mortar interface produce an internal state of stress which consists of tri-axial compression in mortar and biaxial tension coupled with axial compression in bricks. A clear understanding of the strains in brick and mortar at different stages of loading and their relation to the uniaxial response of masonry is not currently available. Proper understanding of the stress states in individual material properties and failure in compression of masonry will lead to improvements in Engineering and design practices.

Results of an experimental investigation of the evolution of strains in the compressive load response of brick, mortar and masonry using digital image correlation (DIC) technique are reported. A finite element model was calibrated using the results and observations of the experimental tests. Using this calibrated finite element model stress states of individual materials in masonry and its failure are studied. It is shown that dilatancy in mortar initiates vertical splitting of brick and final failure in masonry is by splitting of masonry.

An experimental program on the compressive load response of fiber reinforced cementitious matrix (FRCM) wrapped masonry was conducted. The response of masonry, strain states in individual materials and final failure under monotonically increasing compressive forces were obtained using DIC. Using the calibrated finite element model, the effect of FRCM wrapping was investigated. The effect of wrapping is shown to start when mortar exhibits dilatancy. The confinement provided by FRCM is observed to increase the load carrying capacity by limiting the extent of damage in the brick resulting from stabilization of cracks. Final failure produced by the premature failure of FRCM wrapping, which results in a loss of confinement is more brittle when compared to the unwrapped masonry.

Nomenclature

E_b	Youngs modulus of brick
$E_m(\sigma_1, \sigma_3)$	Youngs modulus of mortar as a function of principal stresses
ν_b	Poissons ratio of brick
$\nu_m(\sigma_1, \sigma_3)$	Poissons ratio of mortar as a function of principal stresses
t_b	thickness of brick
t_m	thickness of mortar
$\Delta\sigma_{xb}$	increment of lateral stress in brick
$\Delta\sigma_y$	increment of vertical stress in prism
f_k	characteristic compressive stress of masonry
f_b	normalized mean compressive strength of unit
f_m	normalized mean compressive strength of mortar
$\mu\epsilon$	micro strain
ϵ_{xx}	lateral strain
ϵ_{yy}	vertical strain
f_t	uniaxial tensile strength of the material
τ_c	multiplier to account for tensile stress relaxation
E	Young's modulus of the material
R_t	secant modulus as defined in the figure
ϵ_{ck}	strain at cracking stress
b_t and b_c	shear transfer coefficients

List of Figures

- Fig 1.1** Stresses in brick and mortar when compression is applied on masonry
- Fig 2.1** Stress-strain (longitudinal and lateral) of mortar in triaxial tests.
- Fig 2.2** Effective areas of confinement for different cross sections
- Fig 3.1** Photograph of bricks used in the investigation
- Fig 3.2** Photographs of (a) Mortar; (b) Mortar cylinders
- Fig 3.3** (a) A schematic representation of the masonry column (b) Photograph of the masonry columns
- Fig 3.4** Brick testing experimental setup
- Fig 3.5** Photograph of mortar cylinder test setup
- Fig 3.6** Photograph of the experimental setup for testing masonry
- Fig 3.7** Photographs of (a) brick specimen; and (b) masonry specimen with the sprayed-on speckle pattern
- Fig 3.8** Photograph of the experimental setup with digital camera
- Fig 3.9** Stress-strain plot of brick specimens
- Fig 3.10** Failure of brick specimens
- Fig 3.11** Contour plots of vertical displacement and vertical strain in brick specimen
- Fig 3.12** Strips on loaded image of brick
- Fig 3.13** Stress-strain plot of mortar cylinders
- Fig 3.14** Photograph of the failed mortar specimens
- Fig 3.15** Stress-strain plot of masonry tests
- Fig 3.16** Photographs of the failed masonry specimens

- Fig 3.17** Contour plots of strain in x direction in masonry columns at loads 7.6MPa, 25.35MPa and 40.57MPa
- Fig 3.18** Contour plots of strain in y direction in masonry columns at loads 7.6MPa, 25.35MPa and 40.57MPa
- Fig 3.19** (a) Vertical strips on the loaded image (b) Lateral strips on the loaded image
- Fig 3.20** Variation of ϵ_{yy} along the height of masonry from vertical strip 3
- Fig 3.21** Variation of ϵ_{xx} along the height of masonry from vertical strip 3
- Fig 3.22** Stress vs strain considering lateral strip for mortar
- Fig 3.23** Stress vs strain considering lateral strip at center of brick
- Fig 3.24** Comparison of stress strain behavior of brick and masonry (using DIC), mortar (using extensometer)
- Fig 3.25** Comparison of lateral strain vs axial strain in mortar from DIC and from confined compression tests by McNary and Abrams (1984)
- Fig 4.1** Stack bonded masonry model in ANSYS
- Fig 4.2** Elevation and top view of the model showing boundary conditions
- Fig 4.3** Stress-strain plot of mortar used in MISO model
- Fig 4.4** Graphical representation of failure surface in 3D stress space
- Fig 4.5** Strength of the material in cracked condition
- Fig 4.6** Stress vs strain of masonry
- Fig 4.7** Load response in masonry from experimental test results (red dots shown on the plots are loads at which crack patterns are shown below)
- Fig 4.8** Crack pattern at 39MPa
- Fig 4.9** Crack pattern at 40MPa
- Fig 4.10** Crack pattern at 40.74MPa

- Fig 4.11** (a) stress vs ϵ_{yy} of brick in masonry (b) stress vs ϵ_{xx} of mortar in masonry
- Fig 4.12** Stress vs ϵ_{xx} of mortar in masonry
- Fig 5.1** Photograph of (a) Roll of PBO fiber mesh; and (b) Inorganic matrix
- Fig 5.2** FRCM wrapped masonry specimen ready for testing
- Fig 5.3** Experimental test setup for masonry testing
- Fig 5.4** Stress-strain plot of masonry wrapped specimens
- Fig 5.5** Comparison of stress-strain plot of masonry wrapped and unwrapped specimens
- Fig 5.6** Photograph of (a) Elevation view of failed specimen; (b) Plan view of failed specimen cut at mid-height location
- Fig 5.7** (a) Vertical strips on loaded image (b) Horizontal strips on loaded image
- Fig 5.8** Variation of ϵ_{xx} along the height of masonry from vertical strip 3
- Fig 5.9** Variation of ϵ_{yy} along the height of masonry from vertical strip 3
- Fig 5.10** Stress vs strain in x and y directions of mortar in wrapped masonry from horizontal strip located over the mortar joint
- Fig 5.11** Stress vs strain in x and y directions of brick in wrapped masonry from horizontal strip located over the brick
- Fig 5.12** Comparison of Stress vs ϵ_{xx} in brick from wrapped and unwrapped masonry (from DIC)
- Fig 5.13** Comparison of Stress vs ϵ_{yy} in brick from wrapped and unwrapped masonry (from DIC)
- Fig 5.14** Comparison of Stress vs ϵ_{xx} in mortar from wrapped and unwrapped masonry (from DIC)
- Fig 5.15** Comparison of Stress vs ϵ_{yy} in mortar from wrapped and unwrapped masonry (from DIC)

- Fig 5.16** Link 180 elements used in masonry model
- Fig 5.17** Comparison of stress vs ϵ_{yy} of wrapped and unwrapped masonry from FEM
- Fig 5.18** Comparison of effective strains in the brick from wrapped and unwrapped masonry from FEM (a) stress vs ϵ_{xx} (b) stress vs ϵ_{yy}
- Fig 5.19** Comparison of effective strains in the mortar from wrapped and unwrapped masonry from FEM (a) stress vs ϵ_{xx} (b) stress vs ϵ_{yy}
- Fig 5.23** Crack pattern plan view in a) unwrapped masonry b) wrapped masonry at 39MPa load level
- Fig 5.24** Crack pattern plan view in a) unwrapped masonry b) wrapped masonry at 40MPa load level
- Fig 5.25** Crack pattern plan view in a) unwrapped masonry b) wrapped masonry at 40.74MPa load level
- Fig 5.26** Crack pattern plan view in a) unwrapped masonry b) wrapped masonry at 41.88MPa load level

List of Tables

- Table 4.1** Stress strain data used for mortar in MISO model
- Table 4.2** Elastic material properties of brick and mortar (*directly measured values from brick and mortar, + Inferred from masonry response)

Contents

Declaration	ii
Approval Sheet	Error! Bookmark not defined.
Acknowledgements	iv
Abstract	v
Nomenclature	vi
List of figures	vii
List of tables	x
1 Introduction	1
1.1 Overview.....	1
1.2 Motivation.....	3
1.3 Objective.....	3
1.4 Organization of thesis	4
2 Literature survey	5
2.1 Introduction.....	5
2.2 Compressive Response of Masonry.....	5
2.3 Codal provisons	7
2.4 Application of Digital Image correlation	8
2.5 Fiber Reinforced Polymer wrapping.....	8
3 Test response of stack bonded masonry	10
3.1 Introduction.....	10
3.2 Materials and methods	10
3.2.1 Brick.....	11
3.2.2 Mortar.....	11
3.2.3 Masonry.....	12
3.2.4 Experimental test procedures	13
3.2.4.1 Brick specimen	13
3.2.4.2 Mortar cylinder.....	13
3.2.4.3 Masonry specimen.....	14
3.2.4.4 Digital image correlation.....	15

3.3	Experimental results	16
3.3.1	Brick.....	16
3.3.2	Mortar cylinder.....	19
3.3.3	Masonry specimen	20
3.3	Discussions	26
3.4	Conclusions.....	28
4	Finite element modeling of stack bonded brick masonry.....	29
4.1	Introduction.....	29
4.2	Finite element model	30
4.3	Material models for brick and mortar	31
4.4	Calibration of finite element model	34
4.5	Analysis	35
4.5	Results	35
4.6	Discussions and conclusions.....	39
5	Fiber reinforced cementitious matrix wrapped stack bonded brick masonry	40
5.1	Introduction.....	40
5.2	Materials and methods	40
5.2.1	Fiber reinforced cementitious matrix	41
5.2.2	Wrapped masonry	41
5.2.3	Experimental test procedure.....	42
5.3	Results	43
5.3.1	Test response	43
5.3.2	Digital image correlation	46
5.3.3	Comparison of results of unwrapped masonry specimen and FRCM wrapped masonry specimens.....	49
5.3.4	Finite element analysis of wrapped specimens.....	52
5.4	Summary and conclusions	58
6	Conclusions and recommendations for future work	59
6.1	Conclusions.....	59
6.2	Recommendations for future work	59
	References	61

Chapter 1

Introduction

1.1 Overview

Brick masonry is composite material composed of two materials with different properties: stiffer clay bricks and relatively softer mortar. Mortar placed between bricks along vertical (head) and horizontal (bed) joints bonds the bricks to gather. In structural applications, brick masonry is used primarily as a compression carrying member. Under compressive loads mortar in the bed joint has a larger lateral expansion than the brick. This expansion is confined at the brick–mortar interface by the bricks because of the bond between the two materials. The resulting shear stresses at the brick-mortar interface produce an internal state of stress which consists of tri-axial compression in mortar and biaxial-tension coupled with axial compression in bricks. The stress states in the brick and mortar due to applied compression in the masonry are shown schematically in Figure 1.

Engineered design of masonry structures has evolved largely from construction practice. Standard codes of practice for masonry design specify compressive strength of masonry as a function of unit strengths of brick and mortar, mortar type and mortar proportion. The stress-strain responses of brick and mortar obtained from uniaxial measurements are used as input for simulating the response of the composite, whereas the stress states in the material are clearly multi-axial. A clear understanding of the strains in brick and mortar at different stages of loading and their relation to the uniaxial material response is still evolving. Proper understanding of the stress states in brick and mortar as a function of applied loading, evolution of damage and failure in masonry will lead to improvements in engineering and design practices.

While several studies on the compressive behavior of masonry have been carried out, few detailed investigations on the local interaction between brick and mortar in masonry have been reported. Current understanding of masonry response is based largely on point measurements of strain and visual observations of the recorded damage during the loading process. Failure in masonry is largely attributed to crushing of mortar or cracking of brick. Conventional techniques for strain measurement do not allow for direct determination of strains in the two materials. While, strain measured in the brick and the average strain in the composite are readily accessible, strain field across the surface of the specimen,

which would allow for experimental determination of the interaction between the two materials are not readily available.

In this study, the evolution of strains in individual constituent materials and its relation to the final failure in masonry under monotonically increasing compressive forces are investigated using a full-field optical technique known as digital image correlation (DIC). DIC is a data analysis procedure that uses the mathematical correlation method to analyze digital images of a specimen undergoing deformation. This technique offers the advantage of obtaining spatially continuous measurements of displacements. The results of DIC are used to calibrate a finite element model of the composite material where input for the material constitutive models of brick and mortar are derived from the uniaxial load responses.

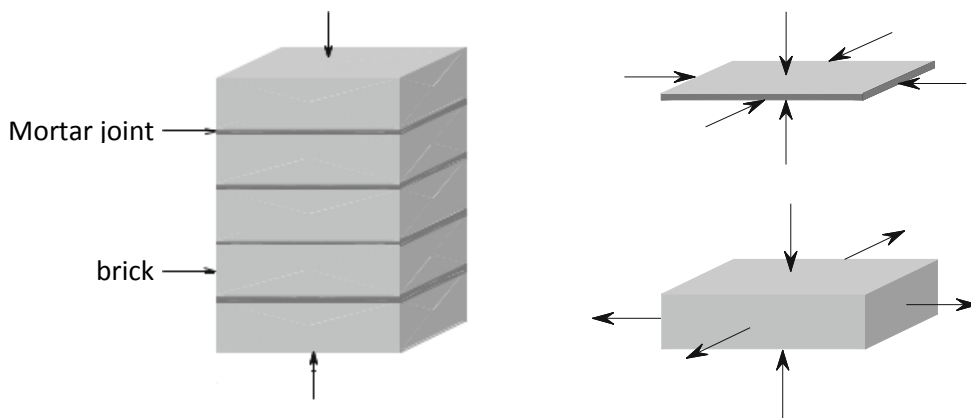


Fig 1.1: Stresses in brick and mortar when compression is applied on masonry

Masonry construction is the most ancient construction practice that is still in use in the modern era. Some of the very old masonry structures still exist with life span of more than hundreds of years. Most of the existing masonry structures were built using available knowledge or as per the available codes of practice. With passage of time the masonry structures are in need of restoration and strengthening as many of the structures have become cultural heritage with a high social value. Considering other factors such as site and local availability of materials many strengthening techniques have been developed and are used in different locations of the world. Recently, fiber reinforced polymer (FRP) strengthening has become a popular material for strengthening as it overcomes several disadvantages of other strengthening techniques. FRP also offers several advantages such as high strength, light weight and ease of application, which makes it a suitable material for use in almost all type of structures. The most common forms of FRP use carbon and glass fibers embedded in a polymeric matrix. Polymers are organic in origin and suffer from extreme sensitivity to moisture, temperature and fire. To overcome these limitations fiber reinforced cementitious matrix (FRCM) composites have recently been developed. FRCM has been

shown to provide outstanding mechanical performance while providing a composite material with performance equal to the conventional FRP composites with epoxy binders.

Significant research has been done on strengthening methods for concrete structures using steel and fiber reinforced polymers (FRP). The use of FRP materials has been proven to especially beneficial in wrapping applications where the confinement provided by the FRP helps increase the load carrying capacity in compression. Wrapping relies on the high tensile strength of FRP to provide confinement to the material. Successful applications of FRP in structural strengthening of concrete columns and piers have been demonstrated. The application of FRCM to strengthening applications is still new and its use in wrapping application for enhancing the compressive strength of masonry columns and piers has not been investigated before. The effectiveness of FRCM in providing confinement needs careful investigation for developing effective strengthening measures using wrapping.

1.2 Motivation

The primary motivation for this study comes from the need to develop strengthening techniques for existing masonry columns and piers in compression. To develop effective strengthening measures requires an understanding of the local material responses of the constituents and the evolution of damage in brick and mortar as a function of the applied stress in masonry. An understanding of the composite response of masonry would also lead to better engineering design procedures and construction practices.

1.3 Objective

The objectives of the research are:

- To study the material response of brick and mortar in stack bonded masonry during the compressive loading using DIC.
- To develop a calibrated finite element model for predicting the load response of masonry
- To study the influence of FRCM wrapping on strain states in brick and mortar and the stress response of masonry.

1.4 Organization of Thesis

The work presented in this thesis is organized in 6 chapters. A brief description of the contents of each chapter is given below

Chapter 2 presents a review of literature related to masonry, DIC and masonry strengthening using Fiber reinforced polymers.

In Chapter 3, the experimental test response of brick, mortar and stack bonded masonry under compressive loading are presented. The results DIC are analyzed to determine the evolution of strains in brick and mortar as a function of applied stress.

Chapter 4 presents details of a finite element model of the stack bonded masonry. Description of finite element model, material models used and the results from the finite element analysis are presented and reviewed.

Chapter 5 presents the experimental test response of fiber reinforced cementitious matrix (FRCM) wrapped brick masonry and its comparison with unwrapped masonry is presented and reviewed. The finite element modeling of FRCM wrapped masonry; its results and comparisons with unwrapped masonry are presented and reviewed.

Summary and conclusions based on the present study are discussed in chapter 6

Chapter 2

Literature survey

2.1 Introduction

In this chapter a review of the literature pertinent to this study is reviewed. Specifically the following topics are covered: Compressive Response of Masonry; Codal Provisions; Application of Digital Image correlation and Fiber reinforced polymer wrapping.

2.2 Compressive Response of Masonry

The first systematic investigation of the strength and deformation of clay unit masonry under uniaxial compressive load was reported by McNary et al. (1985). Biaxial tension-compression tests of bricks and tri-axial compression tests on mortar were performed to establish constitutive relations for each material. Results of this study indicated that behavior of clay-unit masonry could be represented with a simple mathematical model in which the most significant parameter to consider was dilatant behavior of the mortar,

$$\Delta\sigma_{xb} = \frac{\Delta\sigma_y(v_b - \frac{E_b}{E_m(\sigma_1, \sigma_3)}v_m(\sigma_1, \sigma_3))}{(1 + \frac{E_b}{E_m(\sigma_1, \sigma_3)}\frac{t_b}{t_m} - v_b - \frac{E_b}{E_m(\sigma_1, \sigma_3)}\frac{t_b}{t_m}v_m(\sigma_1, \sigma_3))}$$

where, E_b is the Youngs modulus of brick, $E_m(\sigma_1, \sigma_3)$ is the Youngs modulus of mortar as a function of principal stresses, v_b is the Poissons ratio of brick, $v_m(\sigma_1, \sigma_3)$ is Poissons ratio of mortar as a function of principal stresses, t_b and t_m are thickness of brick and mortar respectively, $\Delta\sigma_{xb}$ is the increment of lateral stress in brick and $\Delta\sigma_y$ is the increment of vertical stress in prism.

Vermeltoort et al. (2005) reported that the compressive strength of masonry is not an intrinsic material parameter since failure of masonry is a result of exceeding the tensile strength of the material. The magnitude of the tensile stresses is determined by the geometry of the specimen, and the geometry of real masonry differs significantly from the geometry of test specimens in standard tests. Therefore, failure behavior of masonry cannot be determined by means of standard tests and additional tests are required to

extrapolate the uniaxial behavior to the real three-dimensional behavior. Another reason the behavior of masonry under compression cannot be modeled using results of standard tests is the complex nature of masonry component interaction, a tri-axial stress state occurs under compressive loading.

An empirical relation for the characteristic compressive strength is given in Eurocode 6 as

$$f_k = K f_b^\alpha f_m^\beta$$

where f_k is characteristic compressive stress of masonry in N/mm^2 , K is a constant which varies with type of mortar, α , β are constants, f_b is normalized mean compressive strength of unit in N/mm^2 , f_m is normalized mean compressive strength of mortar in N/mm^2 .

Since masonry is an assemblage of bricks and mortar, it is generally believed that the strength and stiffness of masonry would lie somewhere between that of bricks and mortar. It may be true in cases when one component of masonry, i.e., either bricks or mortar, is substantially weaker and softer than the other, for example, bricks found in the southern part of India are very weak and soft as reported by Dayaratnam (1987) and Sarangapani et al. (2002). Based on an experimental study, Sarangapani et al. (2002) reported that soft bricks (modulus of elasticity —500 MPa) were responsible for development of tri-axial compression in bricks and axial compression with lateral tension in mortar joints of masonry prism. This behavior is contradictory to the generally accepted behavior of the masonry constructed with stiff bricks and softer mortar. From uniaxial compressive tests of brick units, mortar cubes, and masonry prisms constructed with different combinations of bricks and mortar grades masonry prism compressive strength was found to increase with increase in compressive strengths of bricks and mortar. Compressive behavior of mortar with lime was found to be better because of greater ductility; failure strain was about 45% more than that for strong mortar although the compressive strength was about 35% less.

Recently a three dimensional non-linear FE model based on micro-modeling approach to predict masonry prism compressive strength and crack pattern was developed by Vyas et al. (2009). The proposed FE model uses multi-linear stress–strain relationships to model the non-linear behavior of solid masonry unit and the mortar. Willam–Warnke’s five parameter failure theory developed for modeling the tri-axial behavior of concrete has been adopted to model the failure of masonry materials. The crack pattern predicted by this 3D-model developed shows the tensile cracking in prism throughout the height of masonry which means the vertical splitting observed during experimental testing of brick masonry under compressive loads.

Barbosa et al. (2007) tested various bedding mortar samples under tri-axial compression and reported mechanical behavior of mortar under confining stresses. When masonry is subjected to vertical loads,

mechanical interactions between blocks and bedding mortar at the joints induce lateral tension and compression stresses. Mortar specimens of different mixes are tested with application of tri-axial stress state which modifies its mechanical properties and behavior under these confining effects. Out of all mortar mixes, two stronger mortar mixes exhibited ductile behavior and the two weaker mortar mixes exhibited bilinear behavior under high confining pressures. The magnitude and variation of the elastic modulus and poisons ratio are significant in stronger mortar mixes whereas they are not that significant in weaker mortar mixes with the confining pressure.

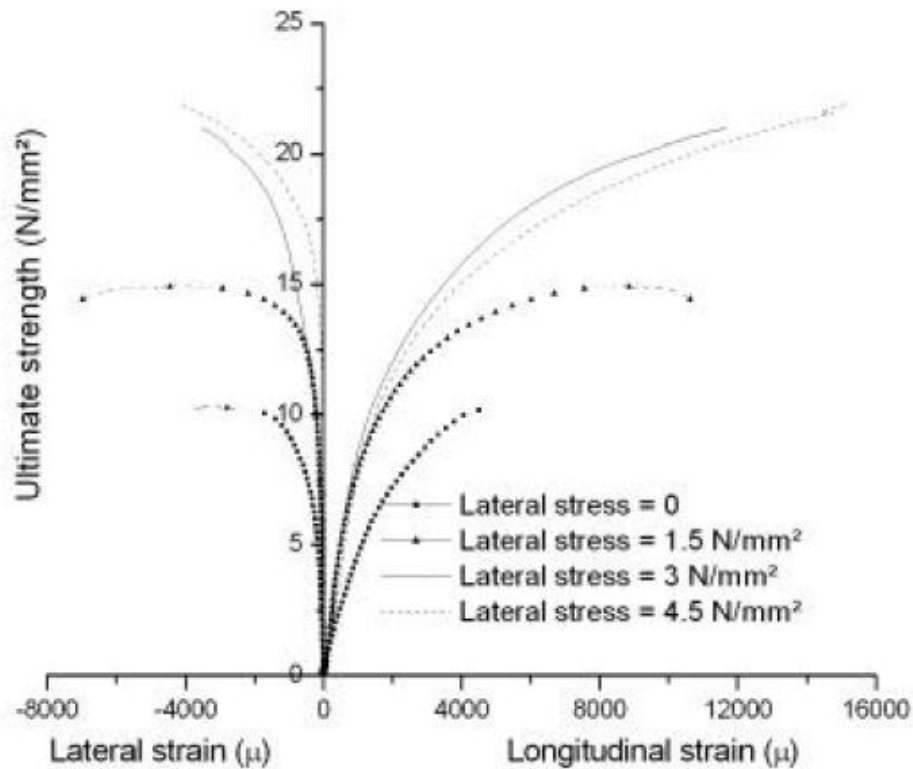


Fig 2.1: Stress-strain (longitudinal and lateral) of mortar in triaxial tests (C.S.Barbosa et al. (2007))

2.3 Codal provisions

Korany et al. (2005) reported the differences and similarities for computing compressive strength of brick masonry, five masonry design codes which includes American 1997 Uniform Building Code (UBC), American 2005 Masonry Standards Joint Committee Code (MSJC), The 2004 Canadian Standards Association Code S304.1 (CSA S304.1), Part 2 of the 2000 British Standard Code (BS 5628), The 2001 Australian Standard Code (AS 3700) and their relevant test standards were compared. The test requirements, the test methods, calculation approach and interpretations are different for different codes

though all these codes used to calculate the same mechanical property. Significant differences were found between the tabulated f'_m values obtained from the different masonry codes: the higher the unit strength, the higher the difference. These large differences suggest that there is still a need for further research to improve our estimate of f'_m based on unit strength and mortar type.

The design approach in IS:1905-1987 is semi-empirical as it combines allowable stress design with traditional rules of thumb for unreinforced masonry only. The compressive strength of the masonry according to Indian standard code IS:1905-1987 is based on crushing strengths of brick and mortar when they are tested individually. Compressive strength of masonry is given by basic compressive stresses (table 8, IS:1905-1987) which depends on strengths of mortar and brick multiplied by various factors such as stress reduction factor, area reduction factor and shape modification factor and has various limitations including slenderness ratios, no eccentricity, height to width ratio. Maximum strength of the brick can be 40MPa which is the upper limit for a typical Indian brick.

2.4 Application of Digital Image Correlation

Carlo Citto et al. extensively used the digital image correlation technique in their experimental investigation to monitor the deformations of various configurations of brick masonry during the shear tests. In the image correlation technique, digital images taken during the test are analyzed and full-field displacement and strain measurement of the tested area. The setup of the system is simple because no contact with the specimen is required. The equipment consists of a digital camera with appropriate resolution connected to a computer for image capturing and save them as tiff images. After the test, the software Vic-2D is used to analyze the images and report the full field displacement and strain measurement. This method tracks the gray value pattern in small neighborhoods called subsets, so random speckle pattern is to be applied to the surface of the specimen for the results. In this experimental investigation, a spray-paint technique where in spray paint is used to produce the speckle pattern on the specimens (coated of white paint first) that need to be tested. Using a digital image correlation technique, the actual vertical strain in the tested brick unit was evaluated and used to calculate the applied compressive stress based on the elastic modulus of the brick and also was used to take a close view of the test method for the in-place measurement of the mortar joint shear strength index.

2.5 Fiber reinforced polymer wrapping

Islam (2008) reported that FRP jackets can significantly increase both the strength and the deformability of masonry under axial load. Ratio of peak stresses of wrapped specimen to that of unwrapped specimen is 3. The effect on ductility is much more when compared to the gain in strength, as the ultimate strain of

confined masonry more than that of unconfined masonry by a factor of more than 30. Under axial loading wrapped square section, the average load increase can be in the order of 34%. If a circular concrete jacket is provided prior to wrapping, load increases averaging 178% due to confinement by the CFRP wrap being effective around the full perimeter of the circular cross section. In most cases, particularly when the cross section aspect ratio was 1, strength and deformability increased almost linearly with the number of layers.

Di Ludovico et.al (2010) investigated FRP wrapping effectiveness on masonry square columns made of clay bricks and tuff bricks through experimental tests. Overall effectiveness of FRP wrapping is more significant in clay bricks when compared to that of tuff bricks. Presence of filled inner core, high porosity and irregularities could reduce the lateral dilation of the column and determine local stress concentration thus making FRP confinement less effective in tuff bricks.

Ascione et.al (2004) stated that the choice of strengthening FRP material should avoid any physical and chemical incompatibility with the existing masonry. The FRP-strengthened masonry walls can prevent the out-of-plane collapse modes due to: overturning, vertical flexure, and horizontal flexure. In these cases, the design of the FRP strengthening is performed through simple equilibrium between the acting forces and the resisting force of FRP strips located on top of the wall to restrain its rotation.

Krevaikas et.al (2005) found that gain in performance of strength and deformability increases almost linearly with the average confining stress from the tests conducted on the wrapped masonry specimens. Increasing the corner radius or decreasing the cross-section aspect ratio is beneficial to the strength and ductility of rectangular masonry columns. Being more deformable, glass fibers are more effective than carbon fibers if the gain in strength and deformability is compared for the same FRP hoop stiffness.

Borri et.al (2011) in their numerical model used the following effective areas of confinement for different aspect ratios of the steel fiber composite wrapped masonry specimens.

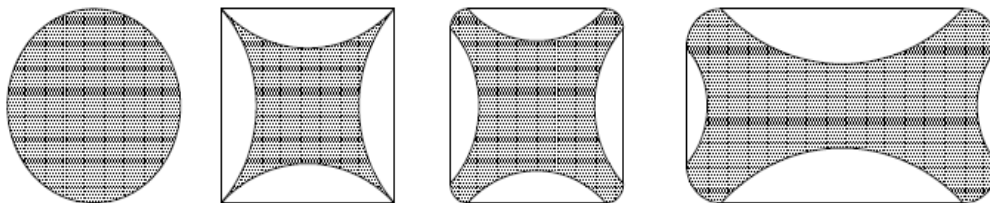


Fig 2.2: Effective areas of confinement for different cross sections (Antonio Borri et.al (2011))

Chapter3

Test response of stack bonded masonry

3.1 Introduction

Brick masonry is a composite material composed of two materials with different properties: stiffer clay bricks and relatively softer mortar. The material response and the failure of masonry in compression depend upon the interaction between the two materials in addition to the relative material properties of the two materials. Deriving the composite response of masonry from the known material responses of brick and mortar requires an understanding of stress states and the associated damage produced in the two materials during the load response. This is often complicated by the geometric variables such as the layout of bricks which depends on the type of bond used. The basic material assemblage in masonry represented by the fundamental repetitive unit represents the spatial variations in materials. Additional complexity is introduced by the range of stress states produced within each material depending on the location within the basic repetitive unit.

In this chapter results of an experimental investigation into the uniaxial compressive response of stack bonded brick masonry are presented. The stack bonded assembly is a very basic sub-assemblage of masonry construction consisting of a vertical stack of bricks bonded with mortar, which allows for studying the influence of mortar and brick on the load response of brick masonry without the added complexity of geometry. The experimental program involved testing of brick, mortar and masonry. In this study, response of masonry, strain states in individual materials and final failure under monotonically increasing compressive forces are investigated using a full-field optical technique known as digital image correlation (DIC). The damage states in the two materials at different stages of loading were investigated and related to the strength, stiffness and deformation capacity of the masonry.

3.2 Materials and methods

In this section, preparation of materials used in the test program and their individual test procedures are reported.

3.2.1 Brick

In current investigation, masonry columns were prepared using hard-fired clay bricks (shown in Figure 3.1) of dimensions: 200mm (length), 90mm (width) and 60mm (height). Smaller coupons were cut from the bricks for material tests to determine the ultimate strength and elastic modulus



Fig 3.1: Photograph of bricks used in the investigation

3.2.2 Mortar

A commercially available mortar premixed, which conformed to ASTM C270 was used (shown in Figure 3.2a). Three mortar cylinders with 150 mm length and 75 mm diameter ($L/D=2$) were cast from the same batch of mortar used to prepare the masonry specimens. Mortar cylinders were used to determine the Elastic modulus and the ultimate strength and are shown in Figure 3.2b.



(a)



(b)

Fig. 3.2: Photographs of (a) Mortar; (b) Mortar cylinders

The mortar was prepared in a standard mortar mixer and the molds were filled in three layers. Each layer was tamped 25 times. After casting the specimens were covered with wet burlap until demolding at 24

hours. After demolding the specimens were cured at 99% RH and 23 deg C for 14 days following which the specimens were stored in the laboratory with environment temperature equal to 23 °C and RH equal to 50% for another 14 days until tested.

3.2.3 Masonry

Masonry specimens used in the test program comprised of stack bonded bricks bonded with mortar. Each model column is composed of 6 bricks with 5 mortar joints in between, as shown in figure 3.3. The thickness of mortar was approximately 12 mm. The cross-sectional area of the specimens tested was 200 mm length, 90 mm width, 372 mm height.

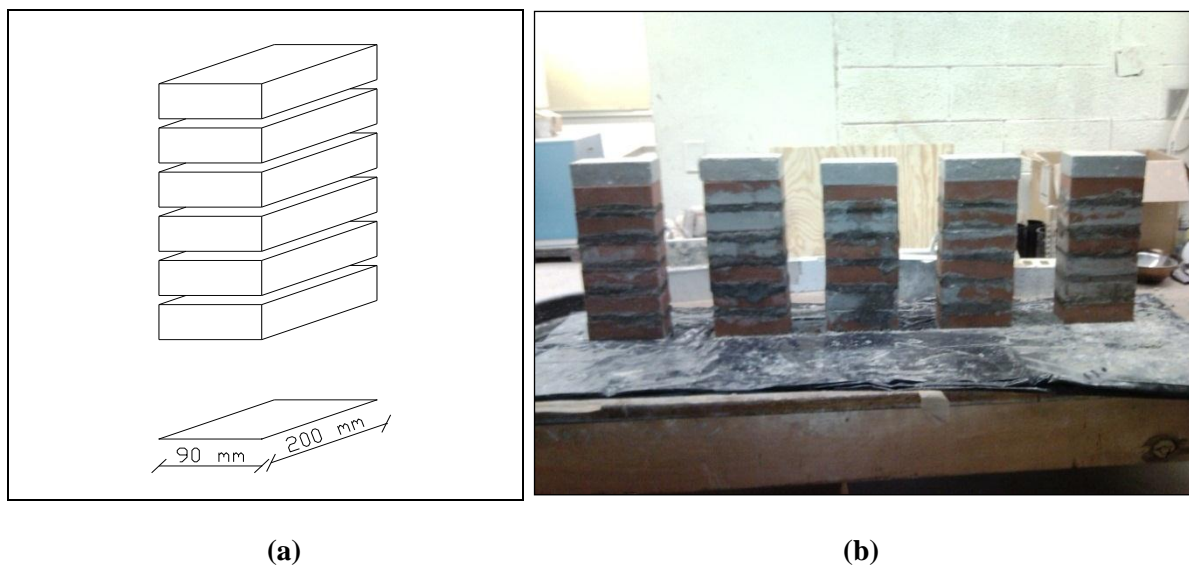


Fig 3.3: (a) A schematic representation of the masonry column; (b) Photograph of the masonry columns

The bricks used in the masonry specimens were stored in an environmental chamber which was maintained at 99% RH for 24 hours before casting. The bricks were removed from the chamber 1 hour before casting and the surface was dried using absorbent cloth. Attention was given to ensure each brick was level before placing mortar. Brick masonry specimens were covered with wet burlap for 24 hours after casting, following which the specimens were cured for 14 days at 99% RH. The specimens were then stored in the laboratory with environment temperature equal to 22 °C and RH equal to 50% for an additional 14 days until tested. A total of 6 brick masonry columns were prepared using clay bricks and were tested under monotonically increasing compressive loads. A photograph of the brick masonry columns is shown in Figure 3.3b.

3.2.4 Experimental test procedures

In this section, experimental test procedures are described.

3.2.4.1 Brick specimen

Bricks specimens of dimensions 95mm length, 45mm width and 60mm height are tested under monotonically increasing compressive loads up to failure. In a typical test compressive load was applied and the platen-to-platen displacement was recorded. Photograph of the loading setup of brick specimen testing is shown in Figure 3.4.



Fig 3.4: brick testing experimental setup

3.2.4.2 Mortar cylinder

Compression test were performed to determine the elastic modulus and the ultimate strength of the mortar. The specimens were fitted with a surface mounted extensometer with a gauge length equal to 12mm and the specimen was subjected to load cycles between 5% and 40% of the ultimate load. The specimens were then unloaded and the extensometer was removed. The specimens were then loaded at a monotonically increasing rate of 110 N/sec up to failure. Only the platen-to-platen displacement was measured when the monotonic load was applied. During the entire loading program, the mortar cylinders were fitted with Neoprene pads at the ends to ensure proper contact between the platen and the specimen. Test setup for mortar cylinder testing is shown in Figure 3.5.



Fig 3.5: Photograph of mortar cylinder test setup

3.2.4.3 Masonry specimen

The stack bonded masonry specimens were tested under monotonically increasing compressive load up to failure. In a typical compressive test load was applied at a fixed constant rate of 6.75kN/minute and the platen-to-platen displacement was recorded. Photograph of the loading setup during a masonry test is shown in Figure 3.6



Fig 3.6: Photograph of the experimental setup for testing masonry

3.2.4.4 Digital Image correlation

In this study, strain states in materials at different stages of loading were investigated using a two dimensional, full-field optical technique known as digital image correlation (DIC). DIC is a data analysis procedure that uses the mathematical correlation method to analyze digital images of a specimen undergoing deformation. This technique offers the advantage of obtaining spatially continuous measurements of displacements. The correlation between the undeformed reference image and the deformed image was used to obtain a two-dimensional displacement field for all points on the specimen surface. The displacement fields were computed through a correlation of gray levels between the reference image and the images of the specimen undergoing deformation using the commercially available software, Vic 2DTM. The strain fields were then computed from the gradients of the displacement field.

Digital image correlation was used for determining the displacement fields at different load levels for brick and masonry specimens. Prior to starting the compression tests, a speckle pattern was created on the surface of the specimens. To create this speckle pattern the specimen is uniformly coated with white paint. The speckle was created by a spray of black paint. Photographs of the brick and the masonry specimens with speckle pattern are shown in Figures 3.7 (a) and (b), respectively.

A reference image of the test specimen was taken after placing it in the test machine, before any load was applied. During the loading process images were taken using a digital camera with a 1Kx1K resolution, which was placed perpendicular to the specimen surface. The images were stored in a computer for analysis. A photograph of the test setup is shown in Figure 3.8. The correlations were performed after the loading was completed. The results of DIC are used to calibrate a finite element model of the composite material where input for the material constitutive models of brick and mortar are derived from the uniaxial load responses.



(a)



(b)

3.7: Photographs of (a) brick specimen; and (b) masonry specimen with the sprayed-on speckle pattern



Fig 3.8: Photograph of the experimental setup with digital camera

3.3 Experimental Results

In this section, testing results of the individual material tests are reported and analyzed.

3.3.1 Brick

In a typical test compressive load was applied on brick and the platen-to-platen displacement was recorded. The compressive load response obtained from three brick specimens is shown in Figure 3.9.

The strain in the figure corresponds to the measured displacement of the platens divided by the height of the brick specimen. It should be noted that the strain obtained from measured platen displacements includes deformation of the spacers (the steel plates used above and below the specimen) in addition to the deformation of the brick specimen.

The measured load response of the brick specimens indicates an essentially linear response up to failure. Failure was produced by splitting of the bricks produced by vertical cracks along the full height of the brick specimen (failed specimens are shown in Figure 3.10). The average value of compressive strength of the brick specimen from the test is 107.42MPa.

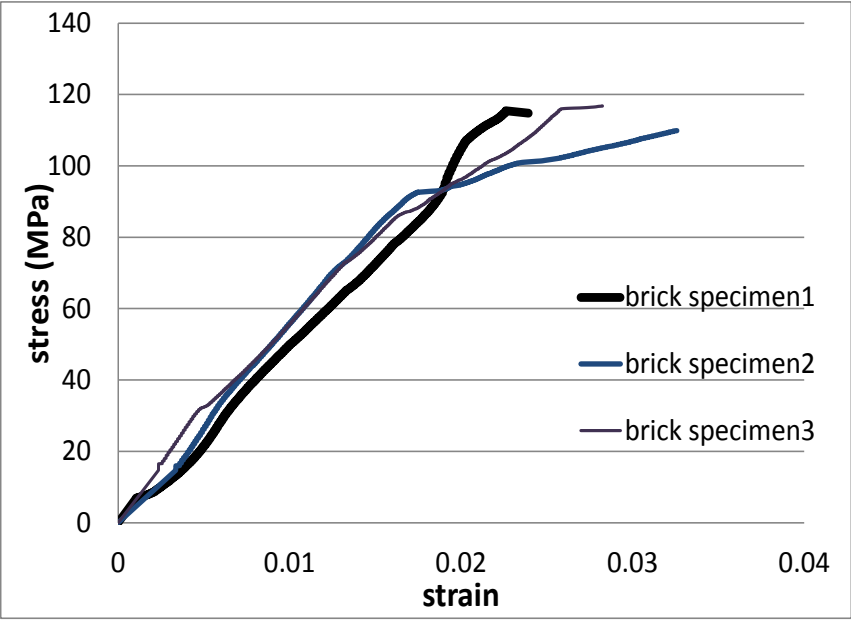


Fig 3.9: stress-strain plot of brick specimens



Fig 3.10: Failure of brick specimens

Images of the surface of the specimen with the surface sprayed speckle pattern were captured at regular intervals of loading. An area of interest measuring 80mm x 45mm, was defined for correlating the images of the undeformed and deformed specimens. The area of interest was defined such that it was removed from the edges and the loading surfaces. A typical result of correlation showing the vertical displacement and the vertical strain in brick specimen at 445kN load level is shown in Fig. 3.11. It can be seen that there is a significant spatial variation in the measured displacement, which is attributed to local material inhomogeneities and temporal noise in the measurements. The variation is significantly higher and more pronounced in the strain, which is derived from the gradient for the displacement. Typical variation in strain is of the order of $100\mu\epsilon$. To remove the influence of local variations in strain from the underlying trends in the measured strains, spatial averaging was used. Strain was averaged over a rectangular area measuring 32mm x 3.8mm as shown in Fig 3.12. The averaged strains from the rectangular strip obtained at different load levels were then used to determine the Young's modulus of the brick. The averaged value of strain measured from the surface of the brick close to failure load was approximately $500\mu\epsilon$. The local fluctuations in strains coupled with the small magnitude of strain produced considerable variation in the measured Young's modulus from one specimen and across specimens. The Young's modulus value for the brick specimen from DIC varied from 61GPa to 93.5GPa.

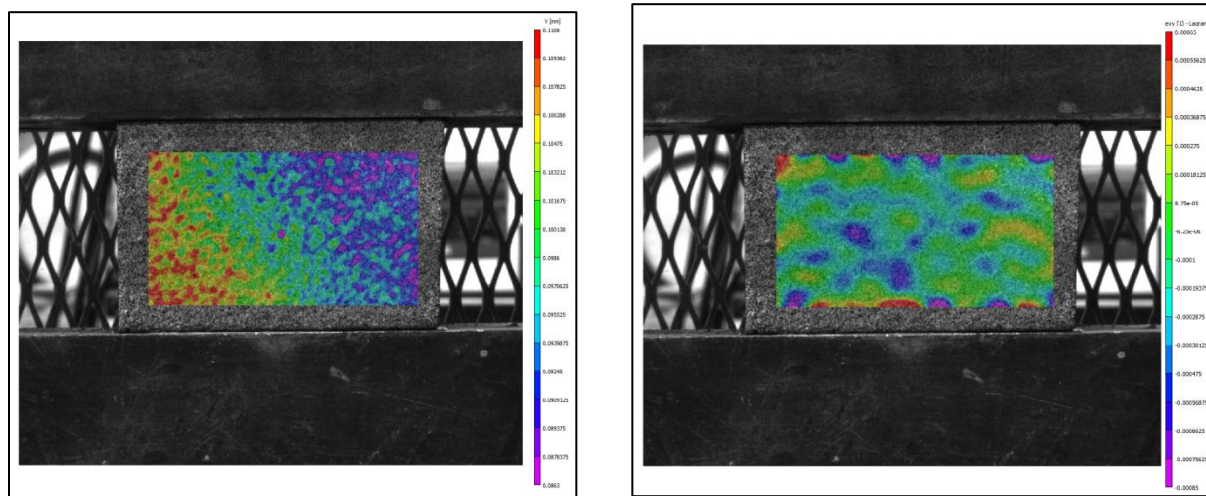


Fig 3.11: Contour plots of vertical displacement and vertical strain in brick specimen

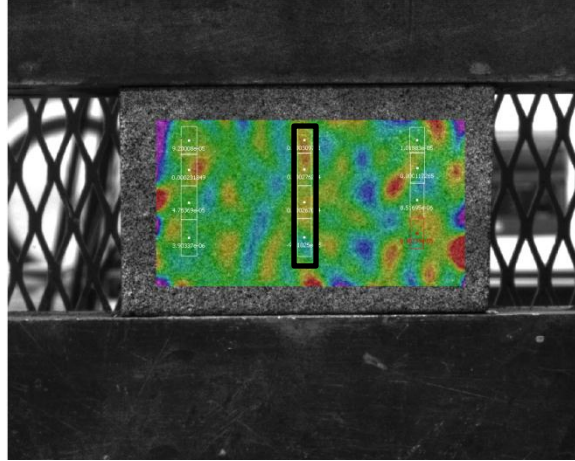


Fig 3.12: Strips on loaded image of brick

3.3.2 Mortar cylinder

Three mortar cylinders of 150 mm height and 75 mm diameter ($L/D=2$) were tested for ultimate strength and Young's modulus. The Young's modulus was measured from the displacement measured by the surface mounted extensometer during the load cycling. The average Young's modulus of mortar was equal to 12.7 GPa (range is 9 GPa to 13 GPa). Stress-strain curves of mortar specimens are shown in Figure 3.13. The strain was computed using the measured platen-to-platen displacements, which was scaled to match with measured strains from the surface mounted extensometer in the early load response. It can be seen that the mortar specimens exhibit significant non-linearity before peak stress. Specimen 3 was found to exhibit premature cracking due to splitting at the neoprene pad which resulted in a low value of compressive strength. Failure in the other two specimens was produced by crushing of mortar and the average value of compressive strengths of these two mortar cylinders is 23.54MPa. A photograph of the failed specimens is shown in Figure 3.14. There is a significant variation in the measured response of the two cylinders. This can be attributed to material variability and to using the scaled values of strain for plotting the stress strain curve. It should be noted that while the scaled strain from platen-to-platen displacements provides an approximate way of accounting for extra displacements, extending the scaling beyond the linear load range is not totally accurate.

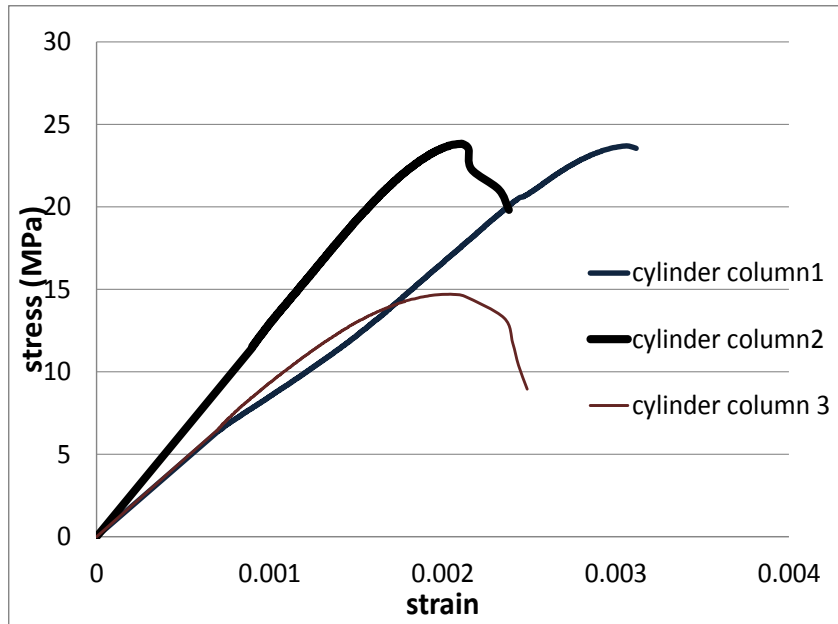


Fig 3.13: Stress-strain plot of mortar cylinders



Fig 3.14: Photograph of the failed mortar specimens.

3.3.3 Masonry specimen

Masonry specimens used in the test program consisted of stack of bricks bonded with mortar. Masonry specimen is tested under increasing compressive loads. A reference image was recorded prior to the start of the loading procedure. Images were recorded, at regular intervals during testing. The platen-to-platen displacements were recorded during the test and used to compute strain. Typical stress-strain response of the masonry specimens are shown in Figure 3.15. It should be noted that the strains in the stress-strain plot include the deformation of the steel platens placed above and below the specimen during testing. The trends in the measured strain indicate an abrupt change in the behavior following an essentially linear

response. The final failure in was produced by splitting of bricks. Since the tests were conducted in load control, failure was found to occur at a very small increment of load beyond the observed change in slope. Signs of distress in the form of cracking sounds were audible close to the end of the linear response and severe cracking was found to occur very quickly in the part of the load response following the linear response. Photographs of the failed specimen are shown in Figure 3.16. The average compressive strength of masonry from the tests is 41.6MPa.

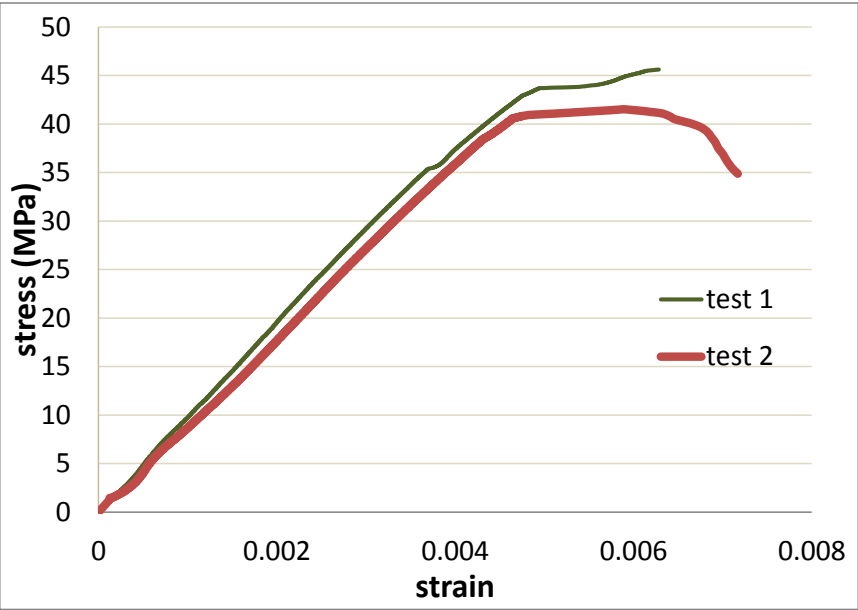


Fig 3.15: Stress-strain plot of masonry tests



Fig 3.16: Photographs of the failed masonry specimens

The correlation between the deformed images and the undeformed reference image was used to obtain a two-dimensional displacement and strain field for all points on the specimen surface. Typical contour

plots of the lateral strain, ϵ_{xx} and the vertical strain, ϵ_{yy} at three distinct points on the load response for specimen 1 are shown in Fig 3.17 and 3.18, respectively. The strains derived from the measured surface displacements exhibit significant local variations and fluctuations, attributed to inhomogeneities, imperfections in the sprayed-on speckle pattern and noise in measurements. These effects are usually amplified further in strains when compared to displacements, since strains are derived from gradients. Despite the local fluctuations, the underlying trends in the measured ϵ_{xx} exhibit no significant variation in between brick and mortar. There is however considerable variation in ϵ_{yy} along the height of the specimen, particularly between brick and mortar. The localization of strain in the mortar joint is evident at 40.57 MPa, which occurs following the initiation of damage indicated by the abrupt change in the load response following the initial linear portion.

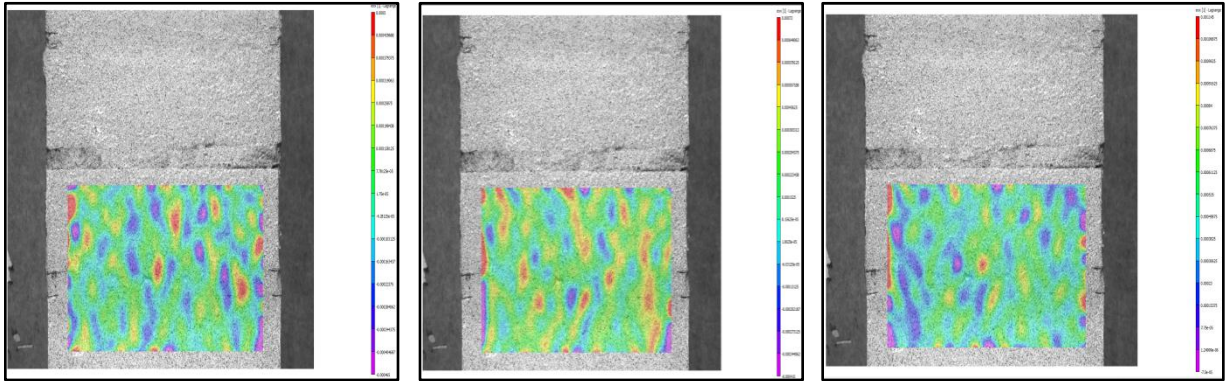


Fig 3.17: Contour plots of strain in x direction in masonry columns at loads 7.6MPa, 25.35MPa and 40.57MPa

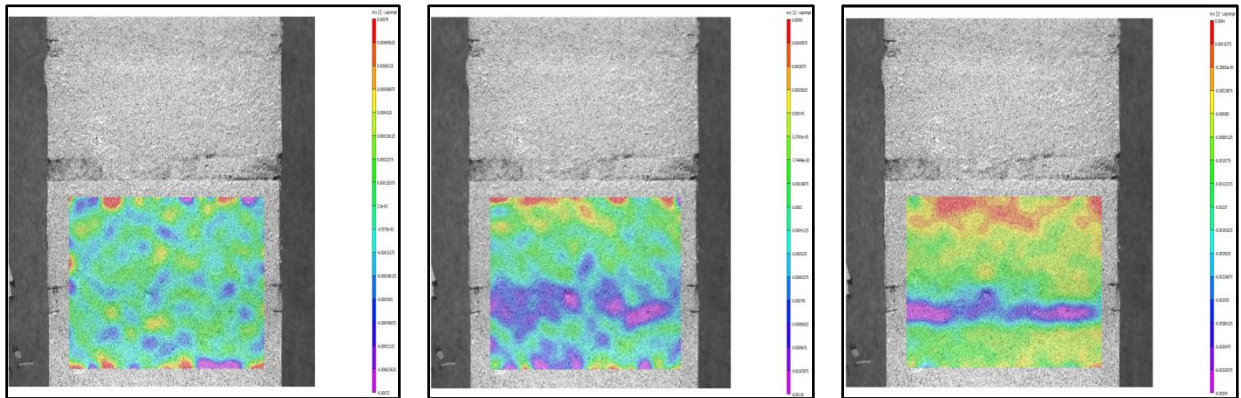


Fig 3.18: Contour plots of strain in y direction in masonry columns at loads 7.6MPa, 25.35MPa and 40.57MPa

Spatial averaging was used for processing the results, in order to clearly identify the underlying trends in the measured strains from the local fluctuations. Horizontal strips of height equal to 11mm were used for

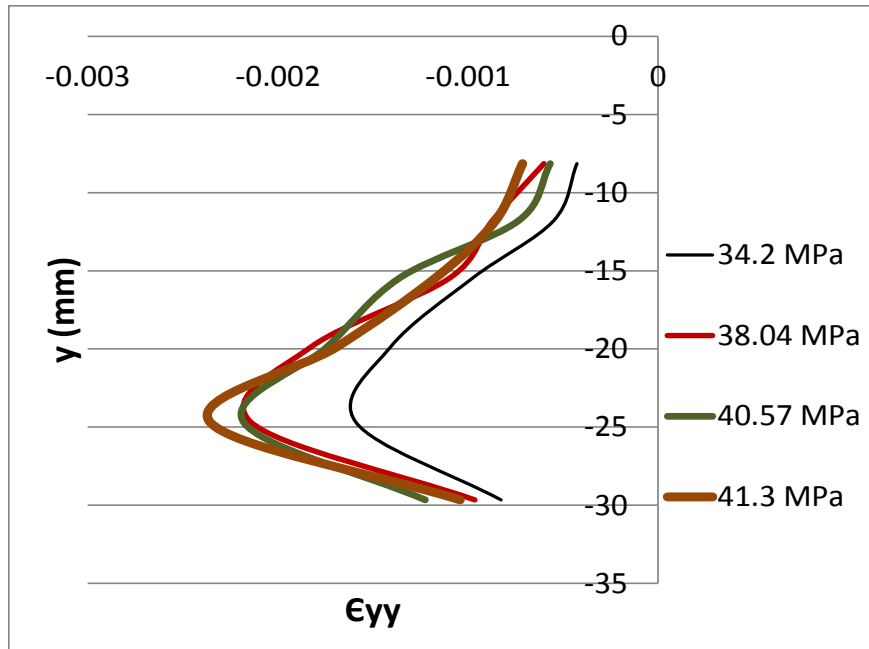


Fig 3.20: Variation of ϵ_{yy} along the height of masonry from vertical strip 3

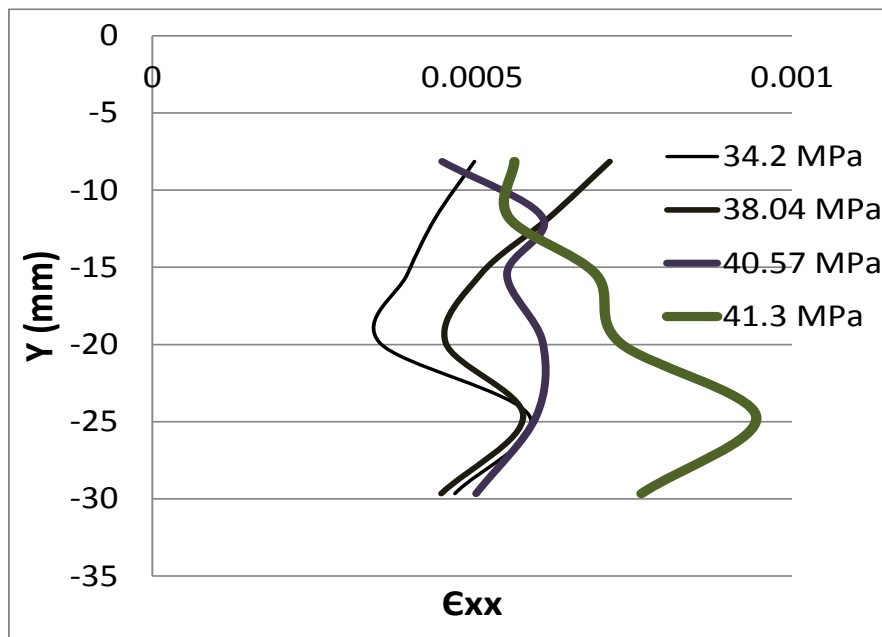


Fig 3.21: Variation of ϵ_{xx} along the height of masonry from vertical strip 3

The strains obtained from the horizontal strips were used in conjunction with the stress calculate from the applied loading to generate the stress-strain response of mortar and brick within masonry as shown in

Figs 3.22 and 3.23, respectively. The plots provide a measure of effective strains considering the multi-axial state of stress in the material. Since mortar experiences confinement in the lateral direction, the measured ϵ_{yy} and ϵ_{xx} correspond to measured strains under applied axial loading with lateral confinement. Similarly, the strains measured from the brick correspond to an applied stress state with lateral tension and axial compression. The effective strains in the brick, shown in Figure 3.22 indicate an essentially linear response up to failure. While the effective strains in the mortar are linear during the linear part of the load response, there is a distinctive change in slope in the measured ϵ_{xx} at the end of the linear load response. There is a larger relative increase in ϵ_{xx} when compared with ϵ_{yy} . This suggests that there is a relatively larger increase in the volume of the mortar during the nonlinear part of the load response. This indicates that mortar exhibits dilatancy prior to failure of masonry.

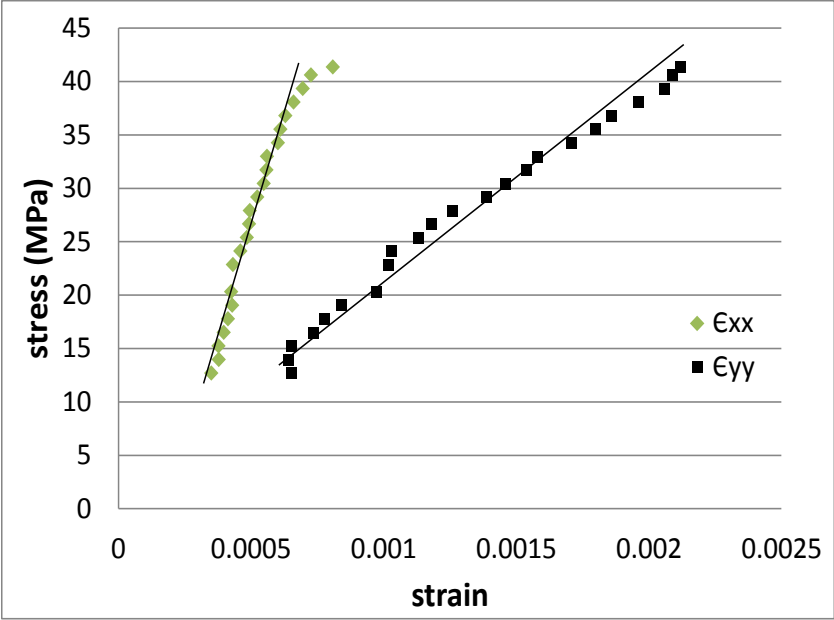


Fig 3.22: Stress vs strain considering lateral strip for mortar

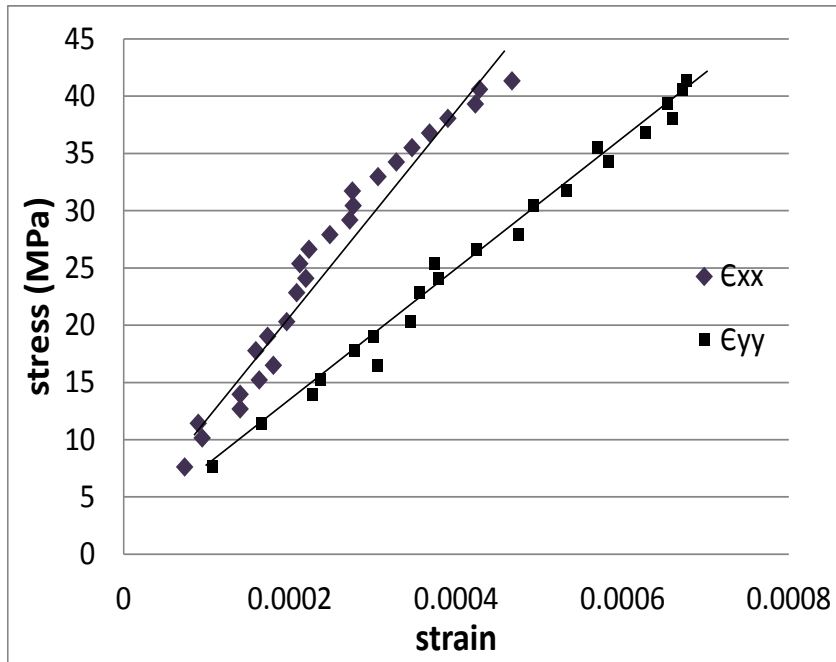


Fig 3.23: Stress vs strain considering lateral strip at center of brick

3.4 Discussion:

A comparison of the stress-strain curves of brick, mortar and masonry is shown in Figure 3.24. The strains obtained from DIC were used in generating the stress strain responses of brick and masonry. The strain used in generating the figure corresponds to the average ϵ_{yy} measured over the entire surface of the specimen. The composite response of masonry is clearly illustrated in the figure. It can be seen that the effective stiffness of the masonry is in between the stiffness of brick and mortar.

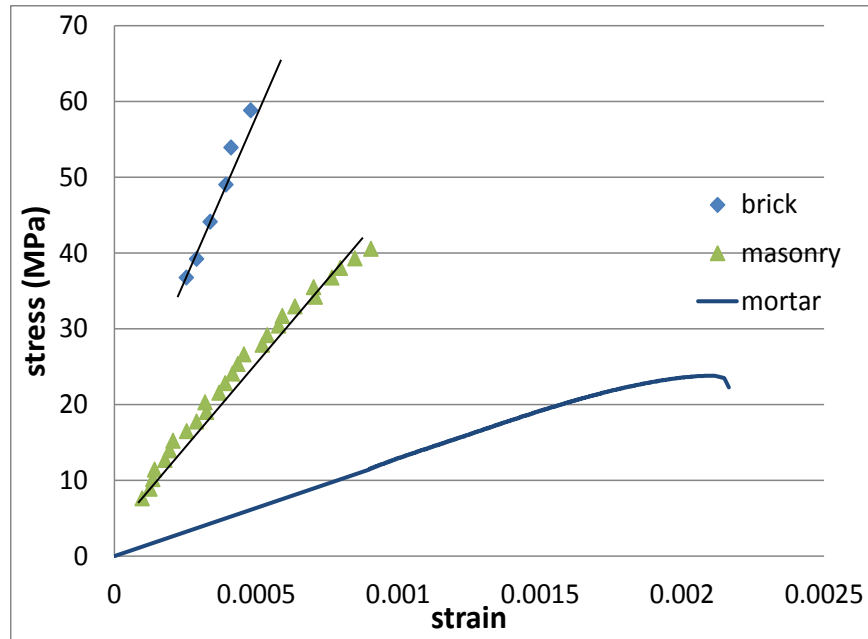


Fig 3.24: Comparison of stress strain behavior of brick and masonry (using DIC), mortar (using extensometer)

The load response and failure in masonry can now be constructed from the observed response of brick and mortar in masonry. From the experimental investigation of brick masonry specimen it is observed that the load response of masonry specimens is linear up to a certain load followed by cracking after which with load remaining constant strains continuous to increase disproportionately. Final failure is by cracking of the whole specimen. The non-linearity in the load response is associated with this dilatant behavior of mortar. As mortar being weaker material becomes dilatant after certain load which in turn imparts increasing tensile stresses on the brick, due to the bond between the two materials as a result specimen fails by splitting of brick. Final failure of the specimen was due to splitting of brick at the joint and there by propagating throughout the height of the masonry.

The dilatant behavior of mortar was earlier observed by McNary and Abrams (1984) in mortar specimens which were tested under applied axial loads at fixed lateral confining pressure. McNary and Abrams suggested that the dilatant behavior of mortar significantly affects failure of the masonry. The dilatant behavior has been measured directly from the masonry specimens in this investigation. This observation is significant since the measurement has been obtained from in-situ conditions, which include the interaction between brick and masonry. It should be noted that unlike in a confined compression test, where the level of confinement remain constant, in the masonry, the level of confinement to the mortar varies as the stiffness of brick changes due to cracking. The findings here confirm that dilatancy in mortar

is responsible for failure of the masonry since it increases the tensile stresses in the brick, causing failure in brick. A comparison of results obtained from mortar within masonry and data from confined tests performed by McNary and Abrams is shown in Figure 3.25.

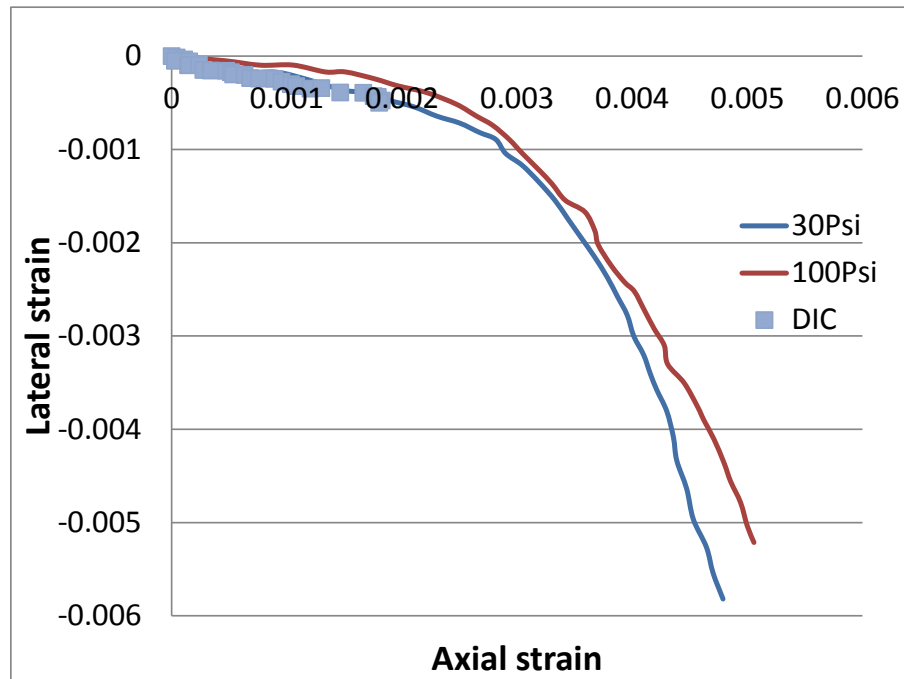


Fig 3.25: Comparison of lateral strain vs axial strain in mortar from DIC and from confined compression tests by McNary and Abrams (1984)

3.5 Conclusions

Based on the work presented in this chapter the following conclusions can be drawn

1. Bricks fail by vertical cracking
2. Failure in mortar is produced by crushing
3. The masonry response in compression is linear up to point which coincides with the onset of dilatancy in mortar. The dilatant expansion of mortar produces failure by splitting of bricks.

Chapter 4

Finite element modeling of stack bonded brick masonry

4.1 Introduction

There have been attempts to predict the compressive response of masonry using material properties derived from uniaxial tests of bricks and mortar. In one of the common approaches used for analysis, which is based on micromodelling, the bricks and mortar are modeled through their respective constitutive laws. Either smeared crack or discrete crack approach is used in the material model for brick. The behaviour of unretrofitted masonry walls can be predicted from the linear elastic stage through cracking and degradation until the complete loss of strength if proper constitutive models for the material are available. Micromodelling strategy is particularly suited for the small scale masonry specimens and structural details where the interaction between the units and mortar is of prime important. The absence of experimental data on the characterization of brick masonry components, however, makes micromodelling of masonry difficult.

The results of digital image correlation (DIC) presented in the previous chapter provided an insight into the response of brick and mortar in masonry and the interaction between the two materials as a function of the applied stress. The measurements from DIC are however confined to measurements on the surface of the specimen. To develop a full understanding of the damage in the two materials as a function of applied loading calibration of a three dimensional finite element (FE) model of the masonry is required. Calibrated finite element model would help understand the interactions between the individual materials.

In this chapter, result of finite element analysis of stack bonded masonry specimens tested in the experimental program is reported. Inputs material properties from brick and mortar were used as input in the FE model for predicting the compressive response of the composite masonry. Material models for predicting triaxial behavior of mortar considering the Willam-Warnke failure theory and orthotropic

damage in brick in the form of a smeared crack model were considered. A three-dimensional FE model was developed for non-linear analysis to predict the load response of masonry and damage in brick and mortar. The response of masonry predicted by the FE analysis provided confirmation of the contributions of brick and mortar to the observed failure in masonry.

4.2 Finite element model

The FE analysis of of stack bonded brick masonry was performed using commercially available finite element software ANSYS™. A finite element model of stack bonded masonry is generated of dimensions 95mm length, 45mm width and 372mm height with six bricks and five mortar joints which is of one fourth of the volume of original masonry tested experimentally. One fourth of the model is considered by cutting across two symmetric planes in x and z-directions to reduce the complexity and computational time for the finite element analysis. Size of the brick and mortar considered in the model are 95mm length, 45mm width, 60mm height and 95mm length, 46mm width 12mm height, respectively. A photograph of the model is shown in the Figure 4.1.

The boundary condition adopted was that all nodes at the base of the models were assumed to be fixed. Symmetric boundary conditions are applied in x and z-directions. Photographs of model showing boundary conditions are shown in Figures 4.2 and 4.3.

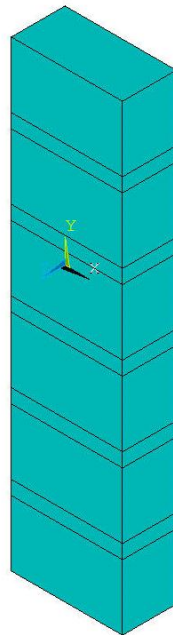


Fig 4.1: Stack bonded masonry model in ANSYS

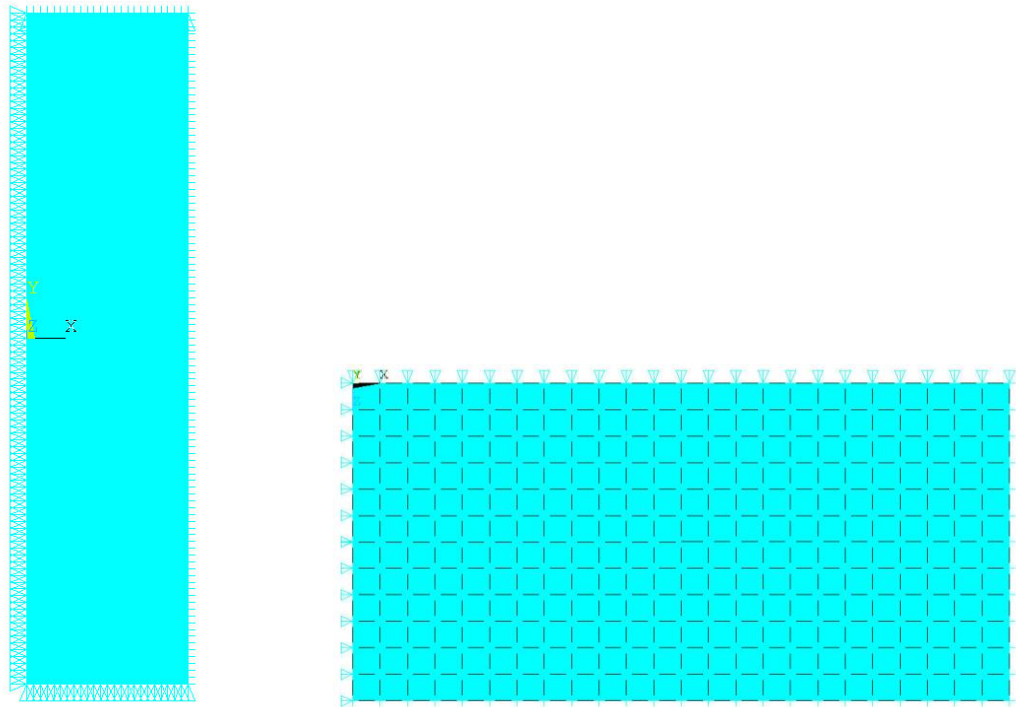


Fig 4.2: Elevation and top view of the model showing boundary conditions

4.3 Material models for brick and mortar

Brick and mortar are modeled using the Solid65 element which has eight nodes with three degrees of freedom at each node; translations in nodal x, y and z directions. Solid65 element supports the capability of simulating damage in concrete in the form of cracking and crushing. Cracking within each element is included in the smeared cracking sense and is permitted in three orthogonal directions at each integration point.

The brick is modeled as a linear elastic material. The mortar is modeled using the multilinear isotropic hardening (MISO) model. The uniaxial stress strain data of the mortar material is given as input for calibrating the MISO model. The stress-strain relationship under multiaxial stress state is derived by matching the equivalent strain with the equivalent stress obtained from the uniaxial stress-strain response. The uniaxial behavior of mortar was described by a piece-wise linear stress-strain curve, with positive stress and strain values. The initial slope of the curve was equal to the elastic modulus of the material. The slope of the stress strain curve is assumed to be zero beyond the last defined stress strain data point. Stress strain data for the piece-wise linear representation of the stress-strain response obtained from tests of mortar cylinders is given in Table 4.1 and the response is shown in Figure 4.3.

Table 4.1: Stress strain data used for mortar in MISO model

stress	strain
0	0
2	0.000157
4	0.000315
6	0.000472
8	0.00063
10	0.000787
12	0.000945
14	0.001102
16	0.00126
18	0.001417
20	0.001575
22	0.001732
22.5	0.00198

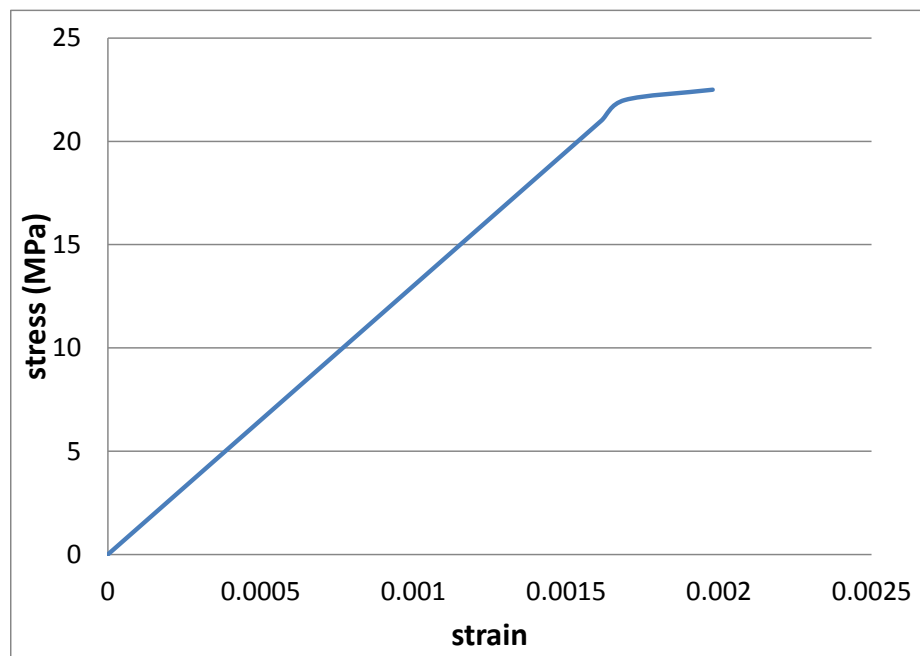


Fig 4.3: Stress-strain plot of mortar used in MISO model

Willam–Warnke failure theory was considered for both brick and mortar. Graphical representation of failure surface in 3D stress space is shown in the Figure 4.4. When the state of stress reaches the critical value given by the Willam-Warnke model the material fails by fracturing or crushing depending upon the state of stress; cracking (tension–tension, compression–tension) and by crushing (compression–compression).

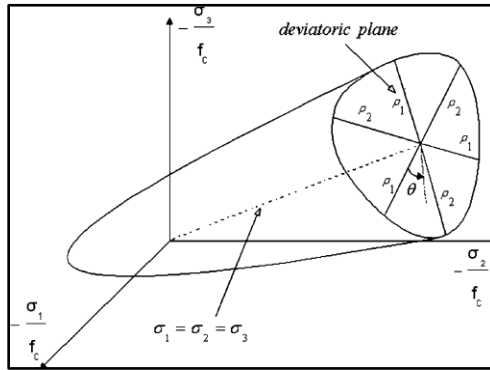


Fig 4.4: Graphical representation of failure surface in 3D stress space

The presence of a crack at an integration point is represented through modification of the stress–strain relationships by introducing a plane of weakness in a direction normal to the crack face. Strength of the material in the cracked condition is represented as shown in Figure 4.5 where f_t = uniaxial tensile strength of the material, τ_c = multiplier to account for tensile stress relaxation, E = Young’s modulus of the material, R_t = secant modulus as defined in the figure and ϵ_{ck} = strain at cracking stress. The shear transfer coefficients b_t and b_c represent the conditions of the crack face. The shear transfer coefficient b_t represents a shear reduction factor for those subsequent loads, which induce sliding across the crack face. The shear transfer coefficient b_t represents conditions of the crack face. The value of b_t ranges from 0.0 to 1.0, with 0.0 representing a smooth crack (complete loss of shear transfer) and 1.0 representing a rough crack (no loss of shear transfer). The superscript c_k signifies the stress–strain relationships referring to a coordinate system parallel to principal stress directions with X^{ck} axis perpendicular to the crack face. If the crack closes, then all compressive stresses normal to the crack plane are transmitted across the crack. This is taken into consideration by introducing a shear transfer coefficient b_c for a closed crack.

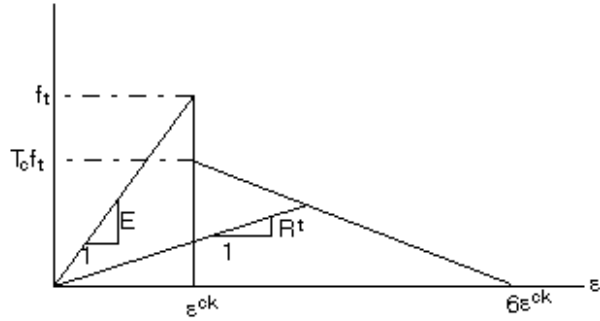


Fig 4.5: Strength of the material in cracked condition

4.4 Calibration of finite element model

Calibration of the finite element model was performed by matching the elastic properties of the composite masonry obtained from the surface measurements from DIC. The experimental data obtained from tests of mortar and brick did not allow for determination of all material parameters needed for the model; the Poisson's ratio of brick and mortar could not be measured directly from material tests. While DIC was used for measuring surface strains in brick during the compression test, the lateral strains could not be determined with sufficient accuracy. The curved surface of the mortar specimen did not permit the use of DIC for strain measurements. In addition, there was a large variability in the measured Young's modulus from the bricks. The unknown elastic material parameters of brick and masonry were determined by using the known value of Young's modulus of mortar obtained from the material test in the FE model of masonry and matching the measured response with the predicted response. The measured response used for determining the three unknown material parameters consisted of the effective material properties of brick and mortar measured from the masonry test. The effective Young's modulus of brick and mortar in masonry were determined from DIC measurements to be 57.8GPa and 17.5GPa, respectively. The effective Poisson's ratio of mortar in masonry was 0.25. The values of Young's modulus of brick, Poisson's ratio of brick and mortar in the FE model were varied till the effective values of the material parameter from DIC matched the FE prediction. The elastic material properties of brick and mortar are shown in Table 4.2.

Table 4.2: Elastic material properties of brick and mortar (*directly measured values from brick and mortar, + Inferred from masonry response)

SI No.	Material	Youngs modulus (MPa)	Compressive strength (MPa)	Poissons ratio
1	Brick	65000 ⁺	107.42*	0.32 ⁺
2	mortar	12700*	23.54*	0.34 ⁺

4.5 Analysis

The load response of the masonry was generated using a displacement control analysis. A displacement boundary condition was prescribed on the top surface while the reaction was measured at the supports at the lower end of the specimen. A displacement increment of 0.001 mm was prescribed.

In the analysis, input parameters for the Willam-Warnke failure surface considered are tensile strength of brick and mortar which were taken equal to 15.6MPa and 3.5MPa, respectively. The crushing property was suppressed for both the materials as it causes instability at an early load. The tensile strength of the mortar is taken as 10% of the compressive strength of the cube. The shear transfer coefficients b_t and b_c used in this study were assumed as 0.2 and 0.5, respectively (standard values from the literature).

4.6 Results

A comparison of the experimental and predicted stress-strain response obtained from the FE analysis is shown in Figure 4.7. The stress in the plot corresponds with the average stress in the cross-section. The strain corresponds to the average strain over the front face of one brick and one mortar joint. The crack patterns in the masonry specimen at three distinctive points on the load response (shown marked on the load response in Fig 4.8) are also shown in Figures 4.9, 4.10 and 4.11. It can be seen that onset of nonlinearity in the load response corresponds with cracking in the brick. Once cracking is initiated, there is significant increase in cracking for a small increment in applied stress. Correspondingly, there is a very small increase in the strains associated with the significant increase in the level of cracking in the brick.

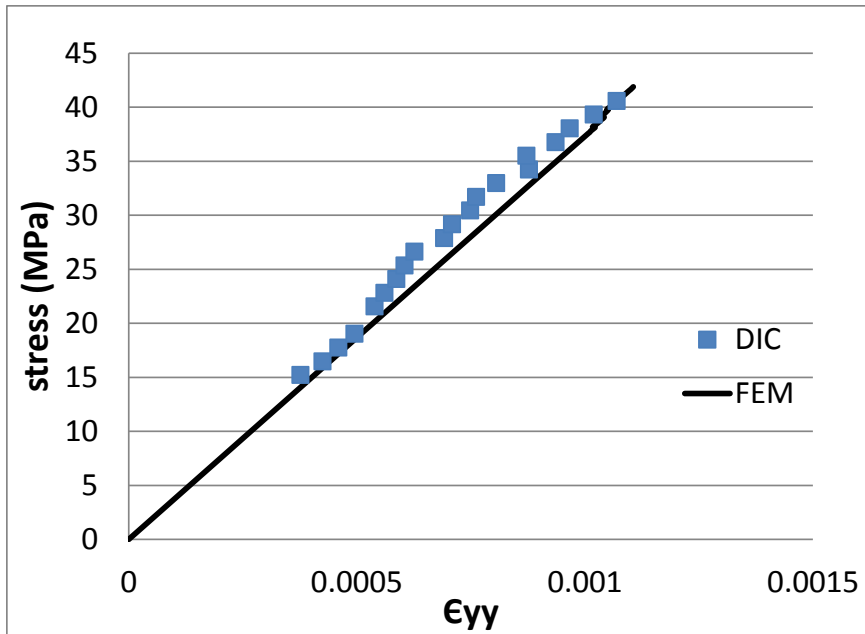


Fig 4.7: Stress vs strain of masonry

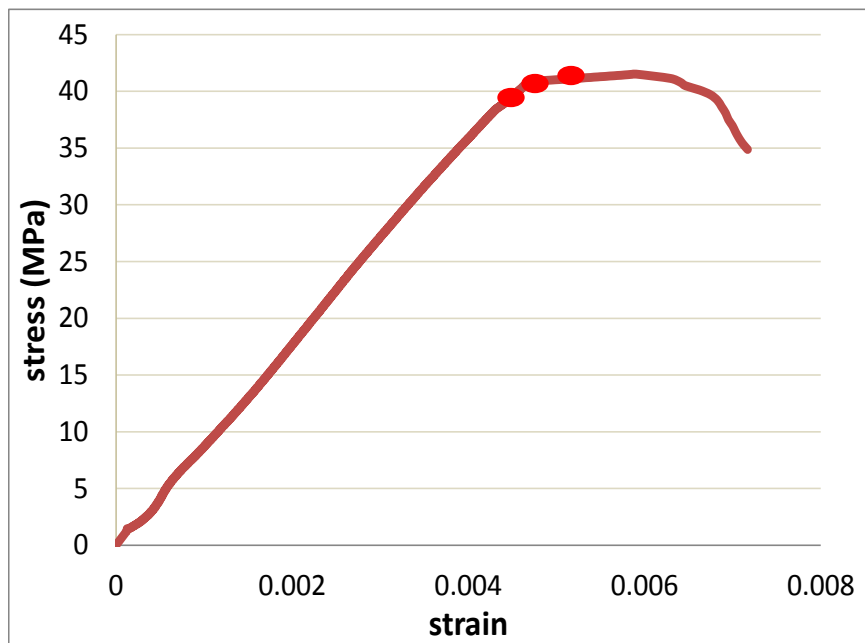


Fig 4.8: Load response in masonry from experimental test results (red dots shown on the plots are loads at which crack patterns are shown below)

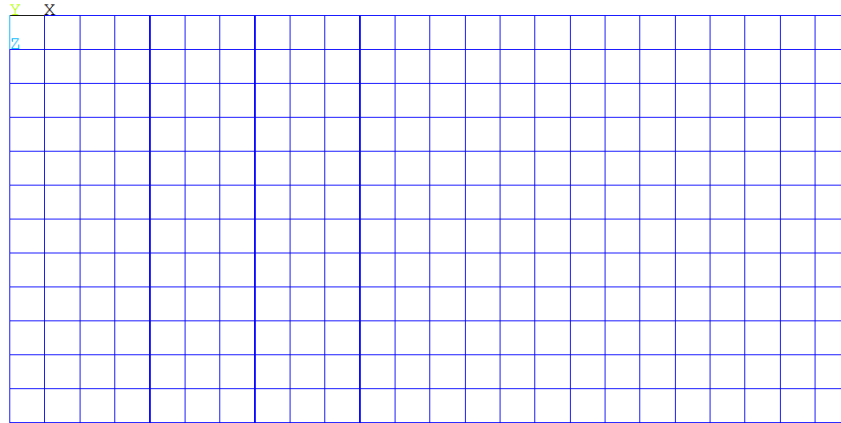


Fig 4.9: Crack pattern at 39MPa

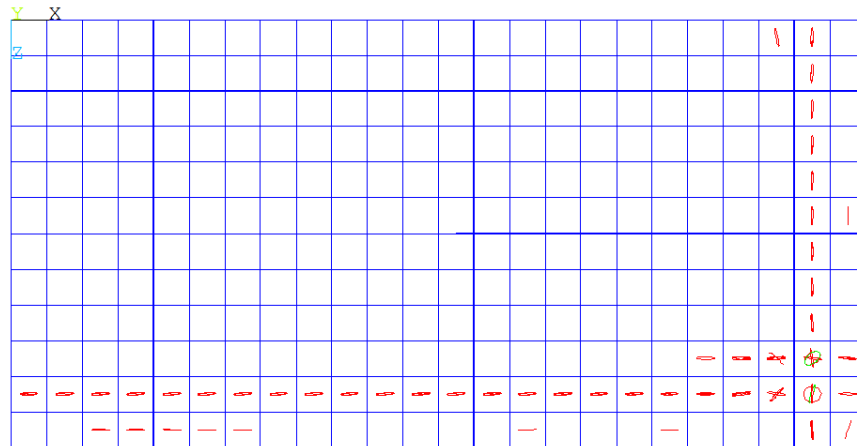


Fig 4.10: Crack pattern at 40MPa

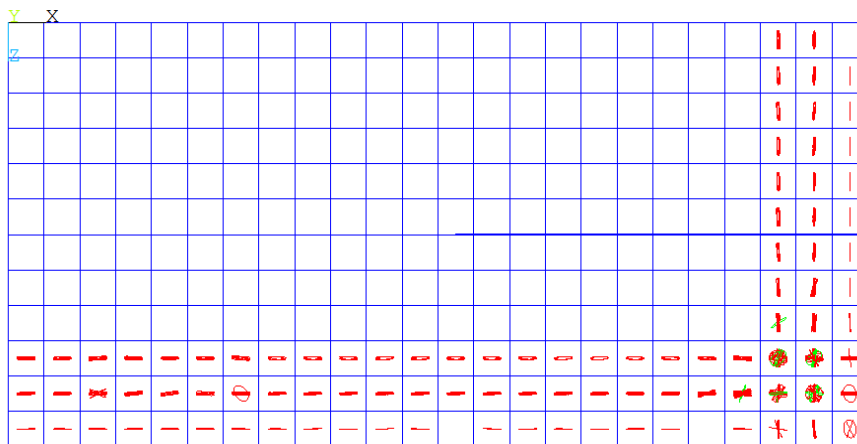


Fig 4.11: Crack pattern at 40.74MPa

A comparison of the ϵ_{yy} in brick and mortar during the loading predicted by FE analysis and obtained from the DIC analysis are shown in Figures 4.12 (a) and (b), respectively. The DIC results obtained from both vertical and horizontal strips are plotted in the figures. The FE analysis predicts an essentially linear response between ϵ_{yy} and stress up to failure, despite the cracking in the brick, which is in agreement with the experimental observation. The response from the mortar exhibits an essentially linear response up to the onset of cracking in the bricks.

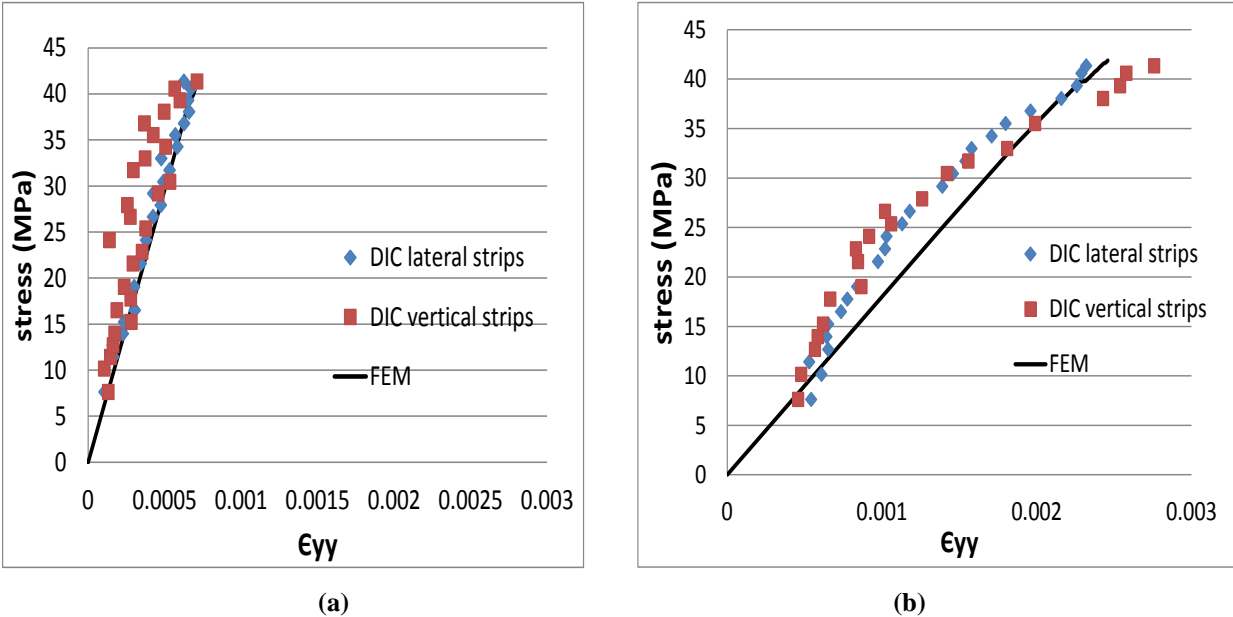


Fig 4.12 (a): Stress vs ϵ_{yy} of brick in masonry (b) stress vs ϵ_{yy} of mortar in masonry

The predicted ϵ_{xx} in the mortar from the FE analysis is shown in Figure 4.13. The dilatancy observed in the mortar response is captured well by the FE analysis. The dilatant response predicted by the FE analysis corresponds with the onset of non-linearity in the load response. The sudden expansion of the mortar also results an increase in tensile cracking in the brick.

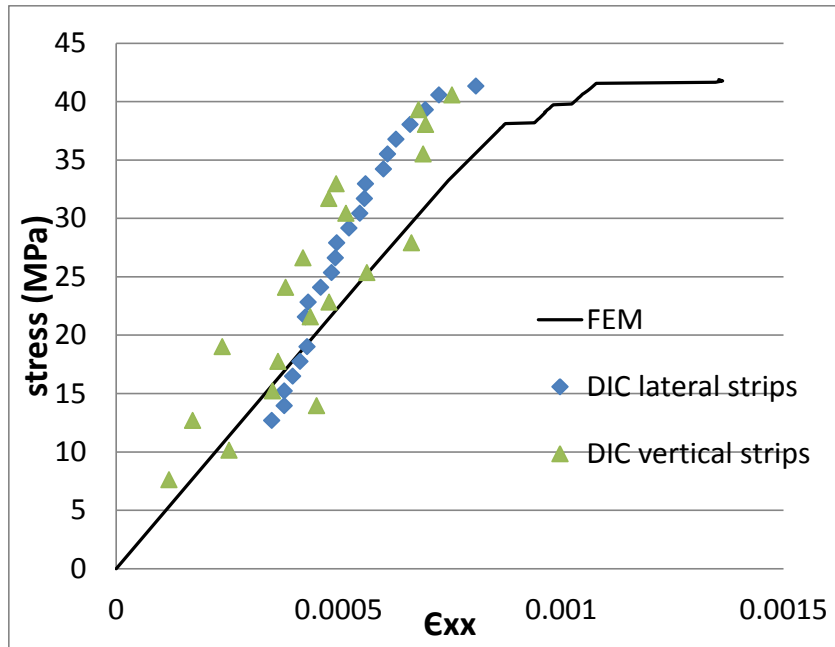


Fig 4.13: Stress vs ϵ_{xx} of mortar in masonry

4.7 Discussions and Conclusions

The response of brick masonry is predicted using the constitutive material behaviors of brick and mortar. The results of FE analysis essentially provide a confirmation of the stress responses of brick and mortar in masonry and the resulting failure in masonry. The failure in masonry is produced by the dilatant behavior exhibited by mortar, which results in increase tensile stress in brick and hence larger cracking. The cracking in brick is associated with an insignificant increase in the measured strain in the masonry. The final failure is produced when the level of cracking in the brick impairs the load carrying capacity of the brick.

Chapter 5

Fiber reinforced cementitious matrix wrapped stack bonded brick masonry

5.1 Introduction

Significant research has been conducted on strengthening methods for concrete structures using steel and fiber reinforced polymers (FRP). The application of FRP for strengthening of masonry structures is however relatively limited. The use of FRP materials has been proven to especially beneficial in wrapping applications where the confinement provided by the FRP helps increase the load carrying capacity of the material. Wrapping relies on the high tensile strength of FRP to provide confinement to the expansion, which is typically observed close to failure in quasi-brittle materials. Successful applications of FRP in structural strengthening of concrete columns and piers have been demonstrated. Ease of installation and light weight make the use of FRP wrapping suitable for applications involving strengthening of masonry piers and columns.

In this chapter, the results of an experimental program on fiber reinforced cementitious matrix (FRCM) wrapped masonry are presented. The experimental load response from the wrapped specimens is compared with the unwrapped specimens. The response of masonry, strain states in individual materials and final failure under monotonically increasing compressive forces are investigated using a full-field optical technique known as digital image correlation (DIC).

5.2 Materials and methods

In this section, properties of FRCM used for wrapping of masonry, preparation of materials used in the test program and experimental test procedure are reported.

5.2.1 Fiber Reinforced Cementitious Matrix

FRCM used in the current study is available under a commercial name “RUREDIL X MESH GOLD” system. This system consists of a Polyparaphenylene benzobisoxazole (PBO) mesh and a stabilized inorganic matrix designed to provide bonding of the the mesh with the substrate. Photographs of the PBO mesh and the inorganic matrix with the commercial name RUREDIL X MESH M750 are shown in Figures 5.1 (a) and (b), respectively. The composite material with the PBO mesh and the inorganic binders have been shown to equal the performance of conventional carbon fiber FRPs with epoxy binders. The PBO mesh reinforced inorganic matrix composites are suitable for reinforcement of masonry, reinforced concrete and pre-compressed reinforced concrete structures and provide superior performance when subject to the simultaneous action of fire and high temperatures.

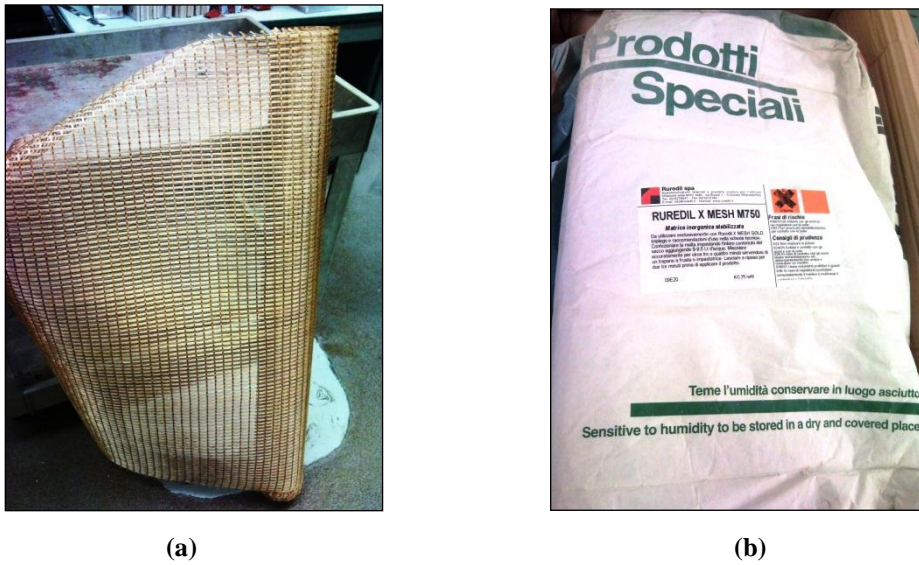


Fig 5.1: Photograph of (a) Roll of PBO fiber mesh; and (b) Inorganic matrix

The equivalent dry fabric thickness of the PBO mesh in the direction of the warp was 0.0455 mm, and the equivalent dry fabric thickness in the direction of the weft was 0.0115 mm. The nominal properties for the PBO fibers are as follows: ultimate tensile stress of the warp per unit of width is 264 kN/m, ultimate tensile stress of the weft per unit of width is 66.5 kN/m and elastic modulus is 270 GPa. The inorganic matrix has a 28 day compressive strength equal to 15 MPa.

5.2.2 Wrapped Brick Masonry

Stack bonded masonry specimens consisting of 6 bricks with 5 mortar joints in between used in the previous experimental investigation were wrapped with one layer of FRCM. The corners of the masonry

specimens were rounded to a radius of 10mm using a grinding machine. For wrapping masonry specimens with FRCM the wet layup procedure was used. In the wet layup procedure, the inorganic matrix is applied on the specimen. A layer of the PBO fibers is placed over the matrix and wrapped tightly around the specimen. The amount of inorganic matrix squeezed out after laying of fibers is removed. In the current experimental study, the FRCM wrapping was prepared with one layer of FRCM which overlapped over a length of 100mm. A photograph of masonry with the FRCM wrapping is shown in Figure 5.2.



Fig 5.2 FRCM wrapped masonry specimen ready for testing

5.2.3 Experimental test procedure

Brick masonry specimens with the FRCM wrapping were tested under monotonically increasing compressive load up to failure. Prior to loading, a speckle pattern was sprayed on the front face of the specimen. Images were recorded, at regular intervals during testing. A photograph of the test setup is shown in Figure 5.3. The platen-to-platen displacements were recorded during the test.



Fig 5.3: Experimental test setup for masonry testing

5.3 Results

In this section, the responses of wrapped masonry specimens and the result of DIC are presented.

5.3.1 Test response

Typical stress-strain response of the masonry specimens are shown in Figure 5.4. It should be noted that the strains were calculated using the platen-to-platen displacement and include the deformation of the steel plates placed above and below the specimen during testing. There is a significant variation in the measured load response and the ultimate load obtained from the three specimens tested. Close examination of the specimens 2 and 3, which failed at low load revealed significant out-of-plane movement resulting from lack of plumb in the specimens. The additional moment induced by the lack of vertical plumb produced a localized crushing in the brick, which resulted in premature failure of the specimen. Only specimen 1 (Column wrapped 1 in Figure 5.4) was considered for further analysis and all subsequent discussion pertaining to wrapped specimens refers to this specimen. The compressive strength of the wrapped specimen is 45.1MPa.

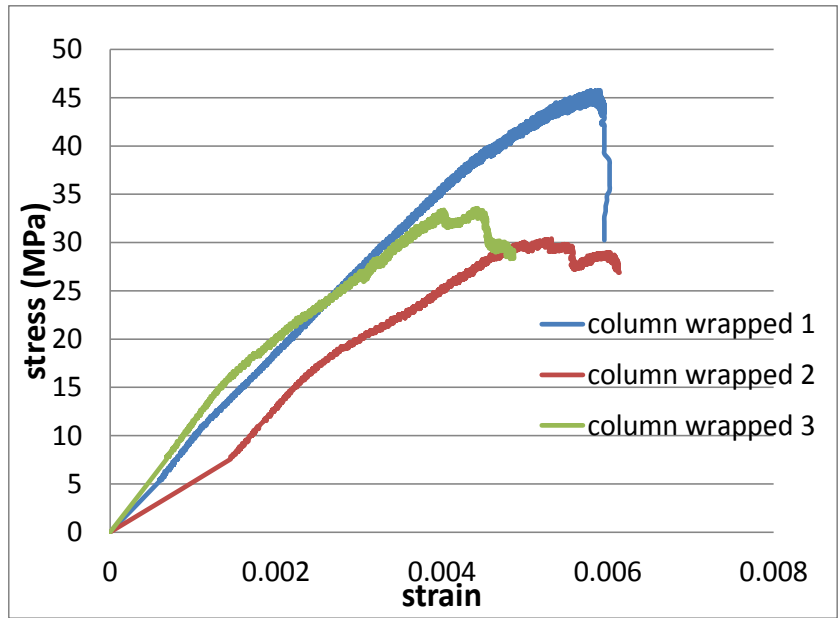


Fig 5.4: stress-strain plot of masonry wrapped specimens

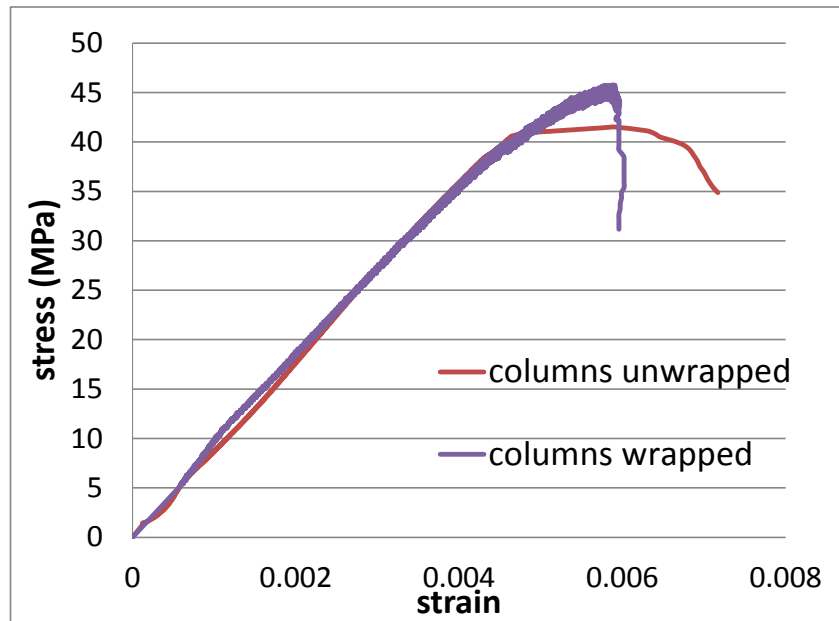


Fig 5.5: Comparison of stress-strain plot of masonry wrapped and unwrapped specimens

A comparison between the load responses of the wrapped and unwrapped specimens is shown in Figure 5.5. It can be seen that there is an increase in the load carrying capacity in wrapped specimen when compared with the unwrapped specimen. The load response of the wrapped specimen is nominally similar to the unwrapped specimen up to a load which corresponds with the initiation of damage in unwrapped specimens. While the load response of the unwrapped specimen indicates an abrupt change in the load

response with an insignificant increase in the load carrying capacity beyond this point, the wrapped specimen continues to support additional load. There is however a marked nonlinearity which is observed in the response of the wrapped specimens as load increases above the initiation of damage in the unwrapped specimens. The final failure in the wrapped specimens was more brittle and occurs at a smaller deformation than the unwrapped specimen.

Failure of the masonry specimen with FRCM wrapping was produced by splitting of the wrap at the location of overlap as shown in the Figure 5.6 (a). Close inspection of the failed specimens revealed the failure in the FRCM occurred due to separation of the two plies over the 100mm lap bonded length. The cross-section of the failed specimen cut at the mid-height location using a wet saw is shown in Figure 5.6(b). It can be noted cracking pattern in the bricks shows distinctive arches along the short sides of brick and a splitting crack parallel to the long side in the middle of the brick. Lifting of the wrap from the specimen in locations close to the middle each side can be seen. The FRCM appears to be bearing with perfect contact at the corners of the bricks. This suggests that the wrapping provides confinement by bearing at the corners while the middle portion of the specimens is not in contact with the wrapping. The failure pattern in the bricks is distinctly different from the observed failure in unwrapped specimens. The failure pattern also indicates that the confinement provided by the wrapping provides forces at the corners, such as typically seen in stirrups in a rectangular reinforced concrete beam [Mander et al. 1988]. This leads to arching action with compression forces directed along a diagonal from the corner. The stresses pattern inside the brick would result in formation of wedges close the ends. The wedges eventually produce splitting of the brick along the length.

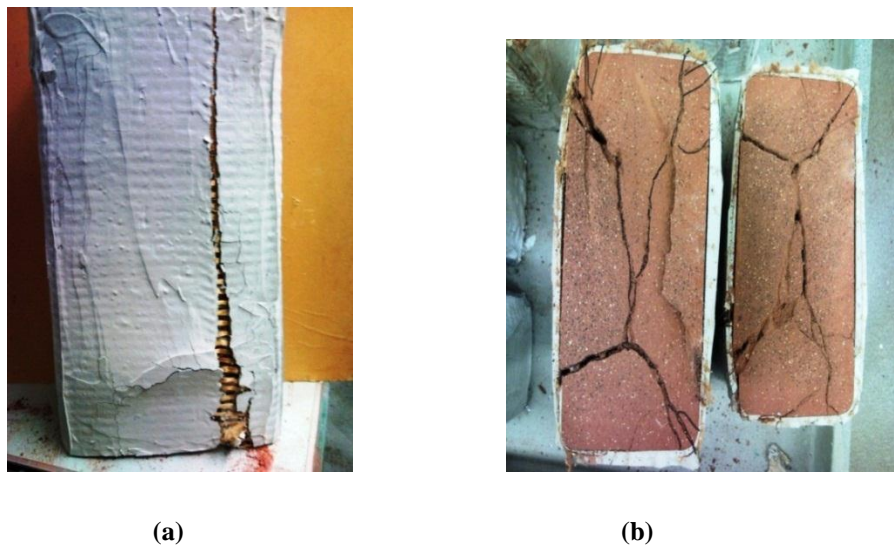


Fig 5.6: Photograph of (a) Elevation view of failed specimen; (b) Plan view of failed specimen cut at mid-height location

Test results indicate that there is no confining effect after loading, until lateral expansion from dilatancy effect is observed. Similar observations had previously been recorded in confined concrete specimens, where the effect of confinement does not increase strength or ductility initially, but when the axial stress is about 60% of the maximum cylinder strength, where concrete starts exhibiting large lateral expansion the concrete is effectively confined [Mander et al. 1988].

5.3.2 Digital image correlation

The procedures developed previously for analyzing the DIC data from the unwrapped specimens was also adopted for the wrapped specimens. Vertical strips of width 6.4 mm were defined at different location across the width of the specimen as shown in Figure 5.7(a). The averaged values of strains over the height of the wrapped masonry specimen from vertical Strip 3 (shown in Figure 5.7(a)) are shown in Figures 5.8 and 5.9. The variations in the measured strains along the height of the wrapped specimen are similar to the observed variations in the unwrapped specimen. High strains alternate with regions of low strains at periodic intervals; the locations of larger strains localization correspond with the mortar joint. There are no significant trends in ϵ_{xx} along the height of the specimen. There is also no noticeable difference in the ϵ_{xx} obtained from the brick and the mortar. The maximum difference in strain along the height of the vertical strip is around $50\mu\epsilon$ which is the accuracy limit of DIC technique.

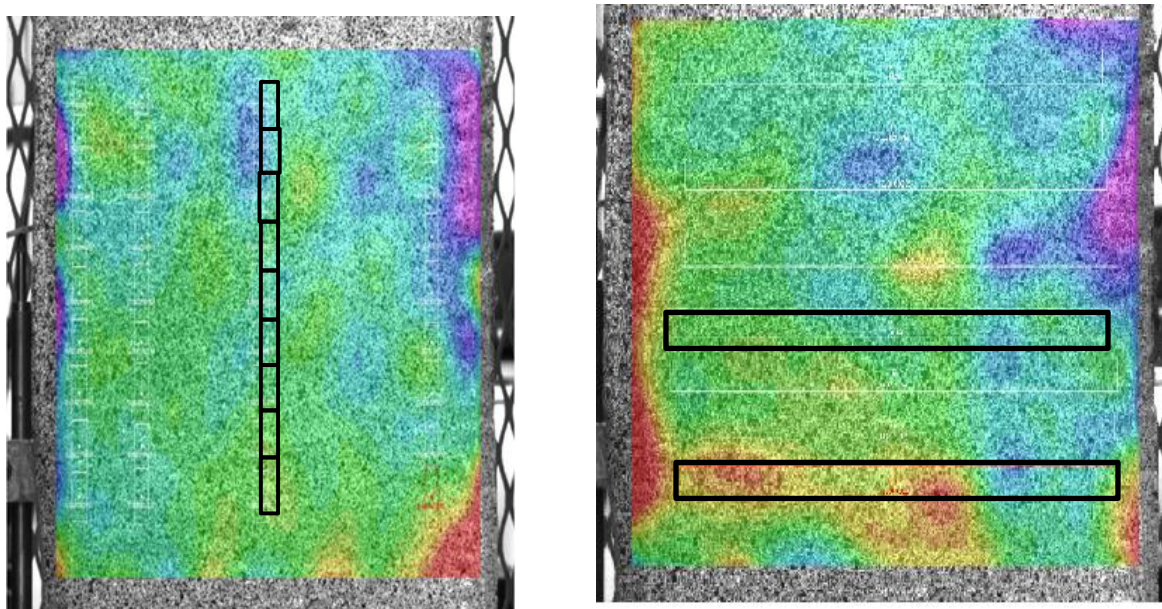


Fig 5.7: (a) Vertical strips on loaded image; (b) Horizontal strips on loaded image

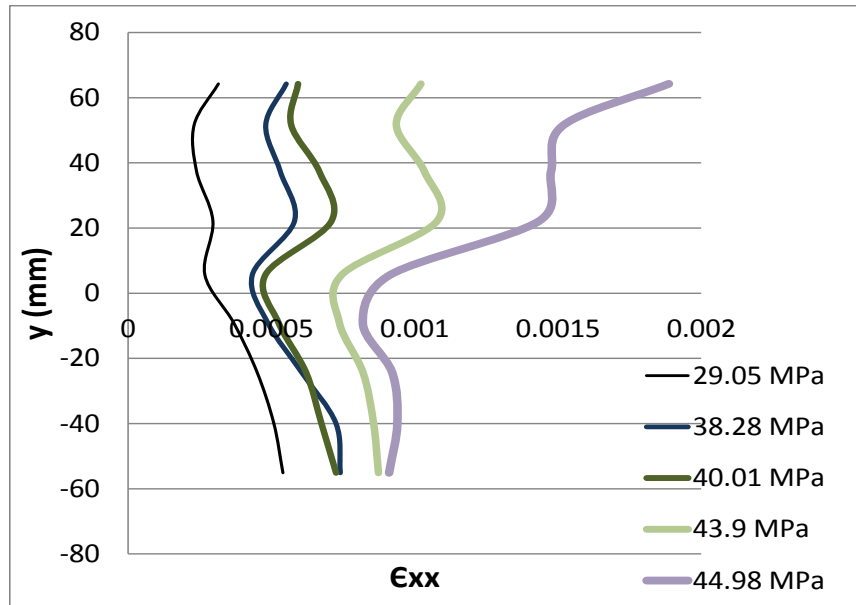


Fig 5.8: Variation of ϵ_{xx} along the height of masonry from vertical strip 3

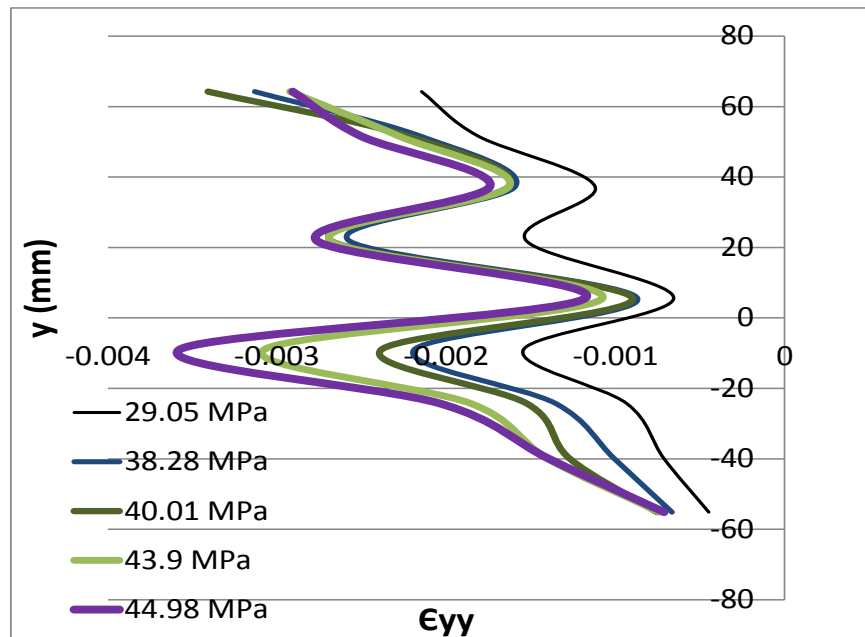


Fig 5.9: Variation of ϵ_{yy} along the height of masonry from vertical strip 3

In wrapped masonry specimen, it is difficult to directly identify the locations of mortar and brick. The measured ϵ_{yy} from the vertical strips were therefore used to identify the locations of the mortar joints. The strains obtained from the horizontal strips located approximately at the center of brick and mortar joint were used in conjunction with the stress calculate from the applied loading to generate the stress-strain response of mortar and brick within masonry and are shown in the Figures 5.10 and 5.11,

respectively. The plots provide a measure of effective strains considering the multi-axial state of stress in the material. Since mortar experiences confinement in the lateral direction from brick and the FRP, the measured ϵ_{yy} and ϵ_{xx} correspond to measured strains under applied axial loading with lateral confinement. Similarly, the strains measured from the brick correspond to an applied stress state with lateral confinement from FRP and axial compression in the vertical direction. The effective ϵ_{yy} in the brick and mortar indicate an essentially linear response up to failure. While the effective ϵ_{xx} in the mortar and brick are linear during the linear part of the load response, there is a distinctive change in slope in the measured ϵ_{xx} at the end of the linear load response. There is a larger relative increase in ϵ_{xx} when compared with ϵ_{yy} in the non-linear part of the load response. This indicates that both brick and mortar exhibit dilatancy at the end of the linear load response.

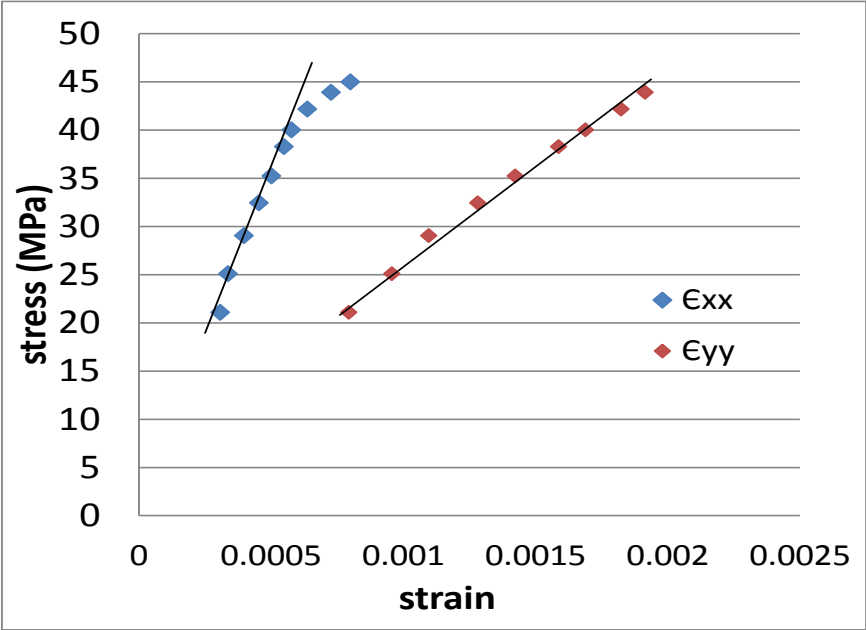


Fig 5.10: Stress vs strain in x and y directions of mortar in wrapped masonry from horizontal strip located over the mortar joint

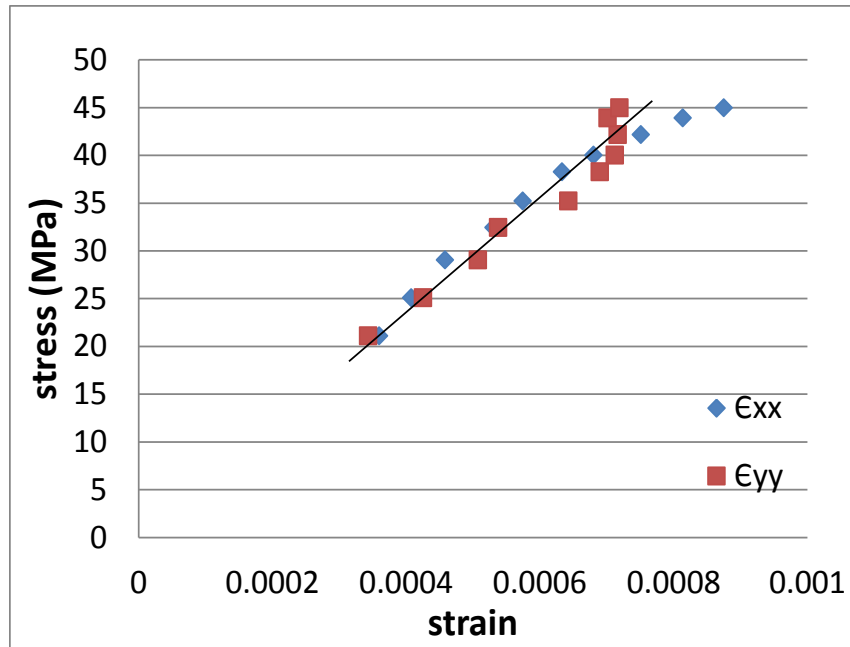


Fig 5.11: Stress vs strain in x and y directions of brick in wrapped masonry from horizontal strip located over the brick

The results of the DIC analysis confirm the observation on the role of FRCM wrapping in providing confinement. A comparison of the load responses of unwrapped and wrapped specimen had indicated that the role of confinement provided by the FRCM is not effective up to the end of the linear part of load response, where mortar exhibits dilatancy in the unwrapped specimens. The measurements from DIC clearly show the dilatancy in the mortar in the non-linear part of the load response of the wrapped specimen. In addition, dilatancy is also observed in the lateral strains measured from the brick. This could be attributed to the internal cracking resulting from the arching action in the brick.

5.3.3 Comparison of unwrapped masonry specimens and FRCM wrapped specimens

Comparison of strains in brick and mortar from wrapped and unwrapped masonry specimens are shown in Figures 5.12 through 5.15. The measured response from the wrapped specimens clearly shows a similar or stiffer response in the measured strains when compared with the unwrapped specimens; the strains in the unwrapped specimens are larger than the strain in the wrapped specimens at any load level. However, the lateral strains in bricks of unwrapped specimens indicate a stiffer response than the wrapped specimen. It should be noted that strains were computed using displacements measured from the surface of the wrapping and not directly on the brick or mortar. These strains are therefore not equal to the strains in the

substitute material. The strains on the surface of the FRCM are reflective of the substrate strain depending upon the quality of the bond and the stiffness of the FRCM. Considering the observed debonding of FRCM across the width of the brick and the bearing at the corners, the measured strains from the FRCM surface represents the average expansion under the influence of bearing at the corners. The different stiffnesses of the FRCM and brick may contribute to a larger ϵ_{xx} measured from FRCM surface when compared to the brick surface in unwrapped specimens. The strains in y-direction measured from the surface of FRCP, however, are reflective of the true behavior of the underlying material substrate since stiffness of wrapping is negligible in longitudinal direction.

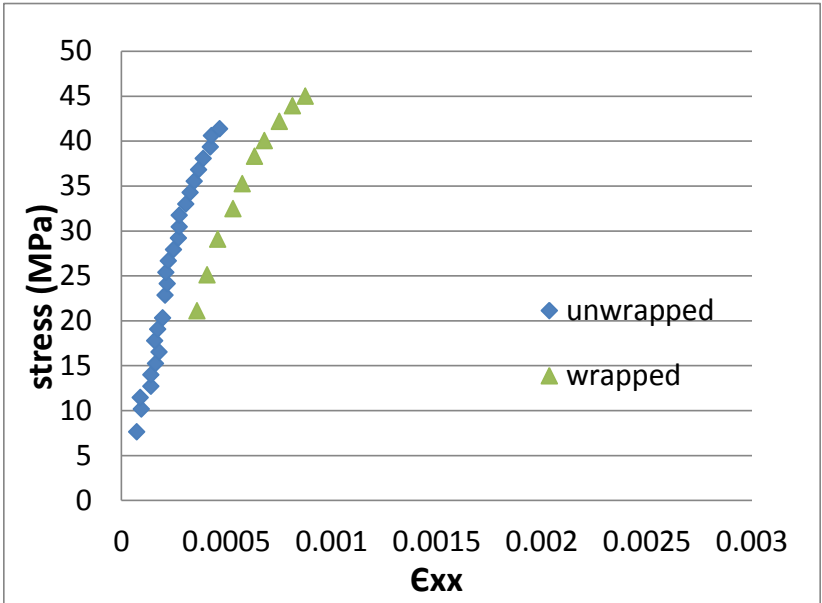


Fig 5.12: Comparison of Stress vs ϵ_{xx} in brick from wrapped and unwrapped masonry (from DIC)

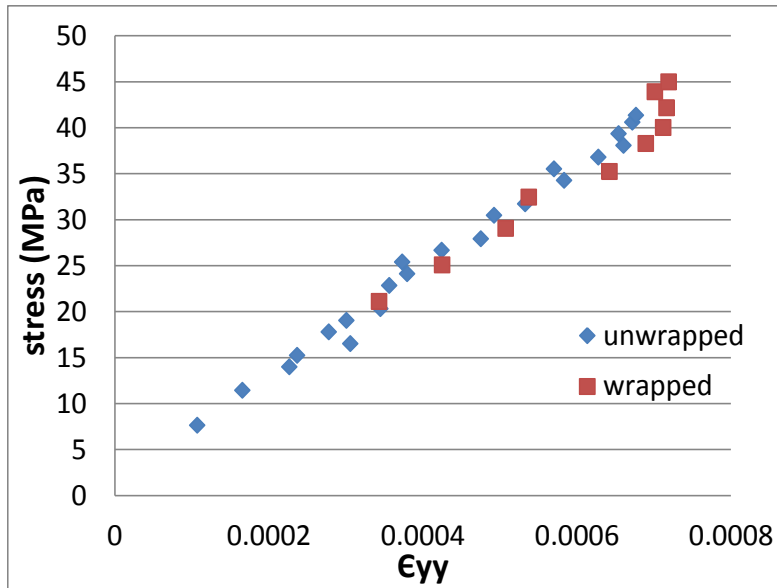


Fig 5.13: Comparison of Stress vs ϵ_{yy} in brick from wrapped and unwrapped masonry (from DIC)

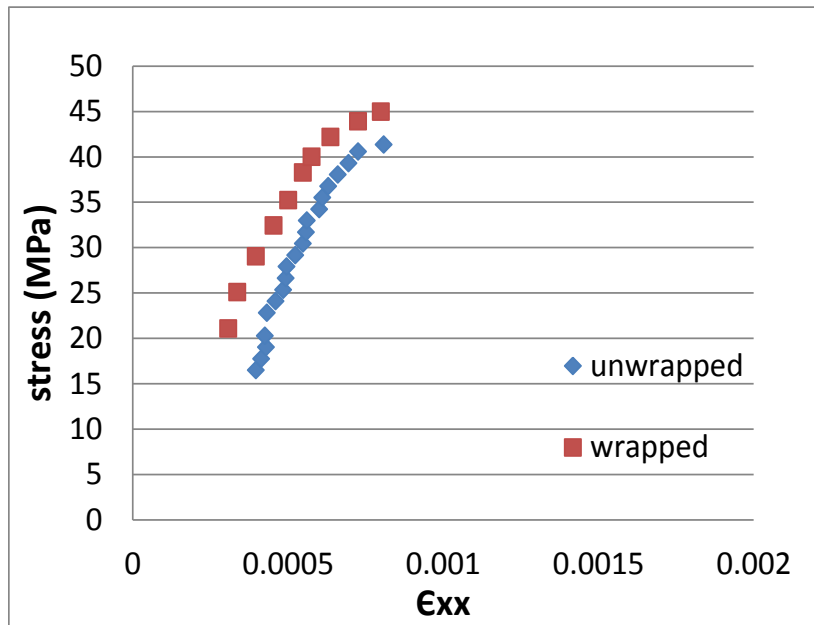


Fig 5.14: Comparison of Stress vs ϵ_{xx} in mortar from wrapped and unwrapped masonry (from DIC)

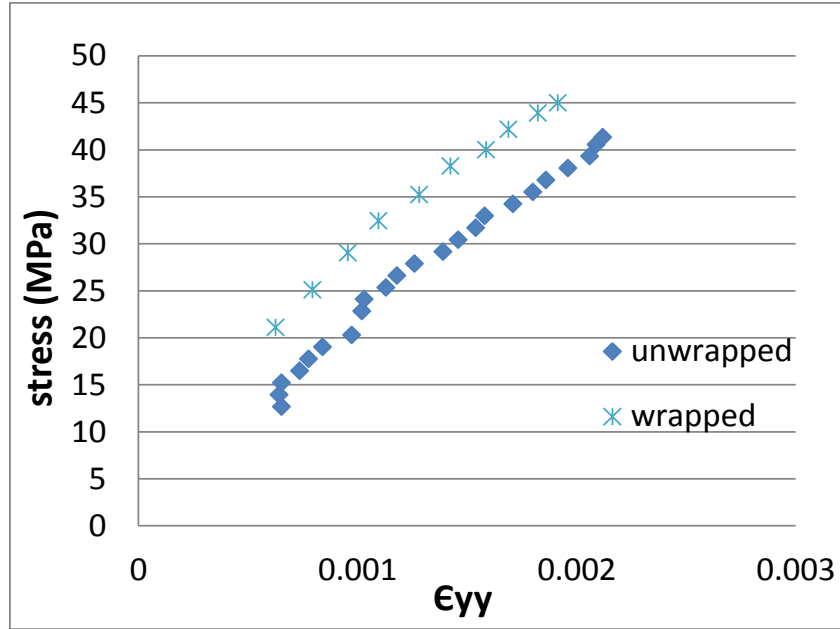


Fig 5.15: Comparison of Stress vs ϵ_{yy} in mortar from wrapped and unwrapped masonry (from DIC)

5.3.4 Finite element analysis of wrapped specimens

Finite element analysis was performed to determine the interaction between the brick and masonry, the role of FRCM in providing confinement and the damage in the materials as a function of the applied stress level in FRCM wrapped specimens. The FE model developed previously was used for masonry. In addition, FRCM wrap was modeled using the Link180 element available within ANSYS. Link180 element is a 3-D spar element which is a uniaxial tension-compression element with three degrees of freedom at each node corresponding to translations in the nodal x, y, and z directions. The tension-only option was activated for link element to model the insignificant stiffness of FRCM under compressive stresses. The link elements were connected to the nodes of the Solid65 elements located at the corners on the front and the side faces of the masonry to simulate the observed lack of bond between the wrap and masonry surface over the central portion of the brick. The link element provides a force which is proportional to the total extension between two nodes located at the corners on the same vertical coordinate. The link elements provide confinement to the total expansion along the two perpendicular faces and bearing at the corner.

A total of 198 elements were used along the height of the masonry model. The cross-sectional area of single link element 0.182mm^2 which is calculated from total cross-sectional area of fibers in the direction of the wrap over the height of one Solid65 element; thickness of the fiber area was 0.045mm and the

height of a single solid65 element (4mm). The FRCM wrap was assumed to be linear elastic with Young's modulus of 270GPa up to failure. A photograph showing link180 elements used in model is shown in Figure 5.16.

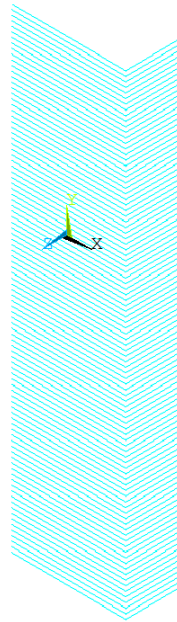


Fig 5.16: Link 180 elements used in masonry model

Displacement controlled analysis is performed with displacement increments of 0.001mm till a stress level of 45MPa was attained. The overall response of the wrapped specimen was obtained by calculating the total reactions generated in response to the prescribed displacements. The responses of constituent materials at different stages of the load response were studied using finite element analysis.

The load response obtained from the FE analysis is plotted in Figure 5.17. The load response from the unwrapped specimen is also plotted in the figure for comparison. The strain in the figure corresponds to the average strain over the surface of one brick and a mortar joint. The results of the FE analyses indicate that there is no difference in load response of the two specimens. While the unwrapped specimen failed at a stress level of 41.8 MPa, the wrapped specimen continued to support additional load beyond 45MPa.

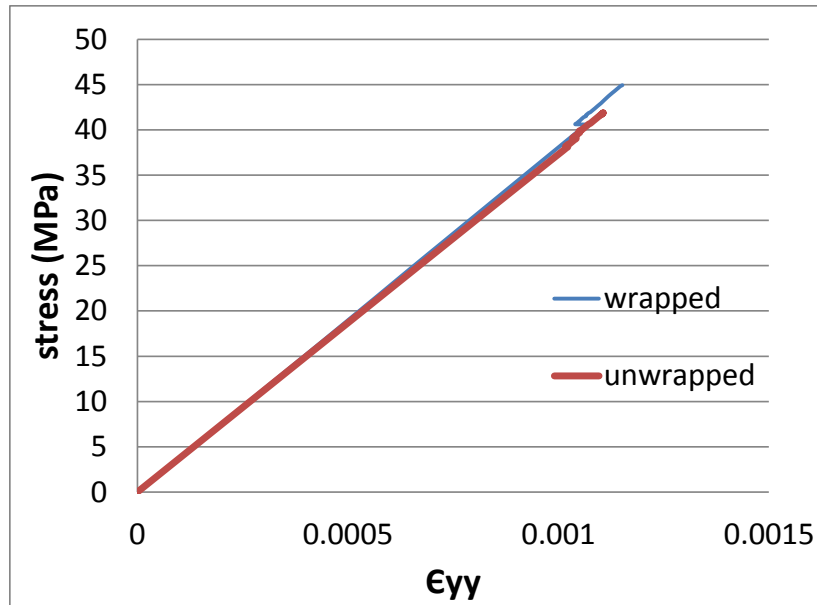


Fig 5.17: Comparison of stress vs ϵ_{yy} of wrapped and unwrapped masonry from FEM

Comparison of the effective strains in the brick for wrapped and unwrapped specimen as a function of the stress level is shown in Figures 5.18 (a) and (b). It can be seen that there is insignificant influence of FRCM on increasing the stiffness of the brick. This suggests that the stiffness of the FRCM is relatively small compared to the stiffness of the brick to provide any significant level of confinement to the brick. In unwrapped specimens there is a slight yet perceptible change in slope associated with the initiation of damage in the brick. The cracking in the brick was observed to coincide with the onset of dilatancy in mortar. There is little or no change in the stress strain response of the brick in the wrapped specimens. This suggests that the damage in the brick is suppressed by the confinement provided by the FRCM.

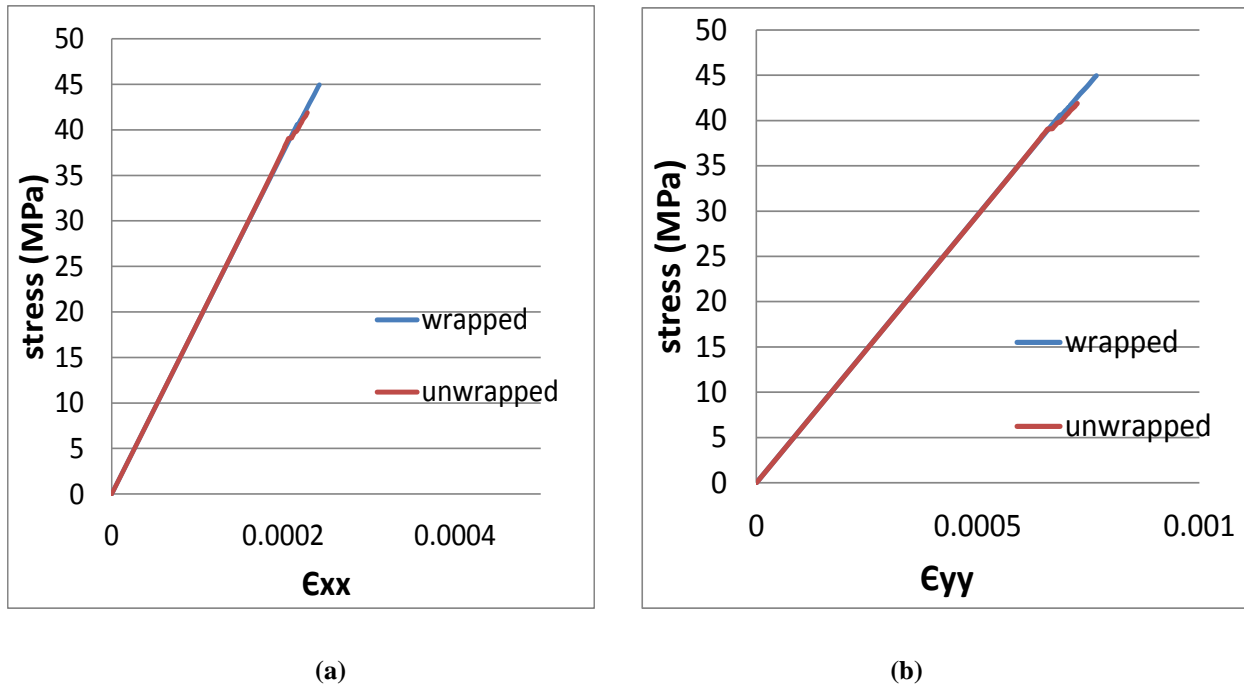


Fig 5.18: Comparison of effective strains in the brick from wrapped and unwrapped masonry from FEM (a) stress vs ϵ_{xx} (b) stress vs ϵ_{yy}

The response of mortar in wrapped and unwrapped specimens is compared in Figures 5.19(a) and (b). The results indicate that wrapping produces an insignificant change in the effective lateral expansion of the mortar before the onset of dilatancy. Dilatancy in wrapped masonry starts at a slightly higher load than the unwrapped specimen. The confinement effect is significant in suppressing the level of expansion produced by dilatancy which results in a stiffened response when compared with unwrapped model at higher stress levels. This indicates a decrease in the tensile demand on the brick reducing the level of cracking for a given applied compressive level.

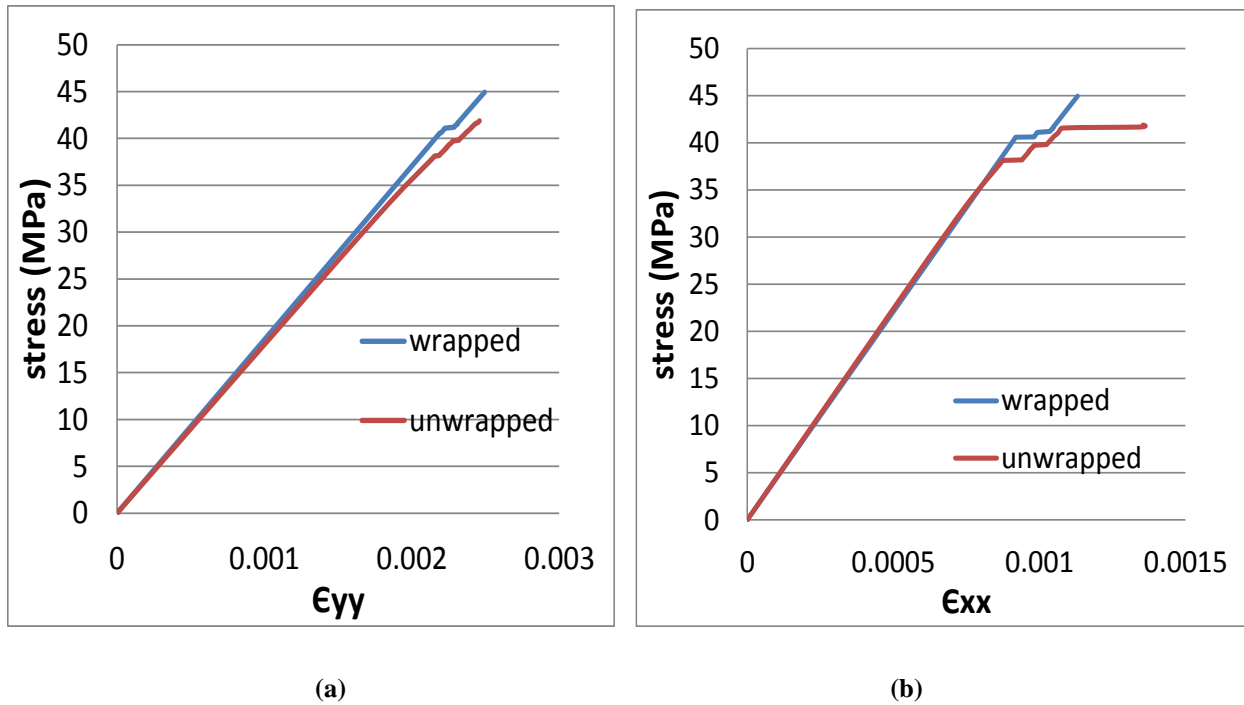
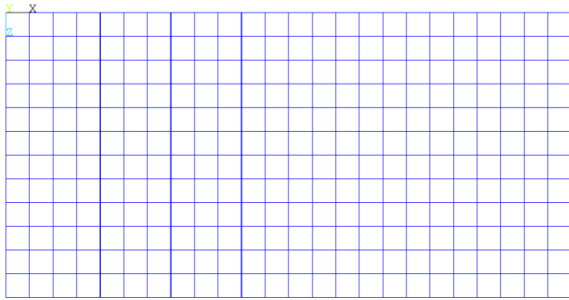
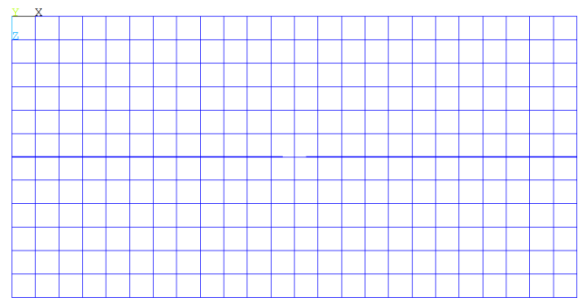


Fig 5.19: Comparison of effective strains in the mortar from wrapped and unwrapped masonry from FEM (a) stress vs ϵ_{xx} (b) stress vs ϵ_{yy}

Crack patterns obtained from finite element analysis of both wrapped and unwrapped masonry models at different load levels are shown in Figures 5.20 through 5.23. The crack patterns are shown for a load level just prior to and after the onset of dilatancy in the unwrapped specimen. The crack patterns essentially confirm the observations from the individual strain responses of brick and mortar. Cracking in the brick occurs at a higher load than the wrapped specimen. At any stress level there is significantly lower level of damage in the wrapped specimen when compared with unwrapped specimens. With increasing load, there is a progressive increase in extent of cracking in the unwrapped specimens. In the wrapped specimens, the extent of cracking appears to stabilize with increasing load. Therefore the confinement provided by FRCM decreases the level of dilatancy of mortar, reducing the tensile demand on the brick, which results in a decrease in the level of damage in brick.

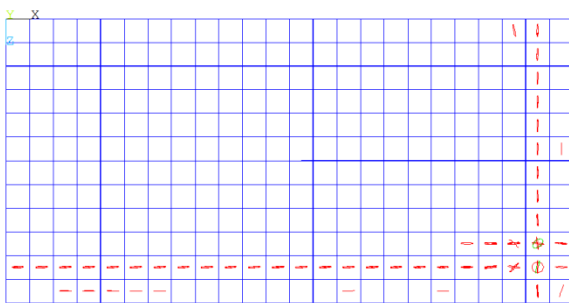


(a)

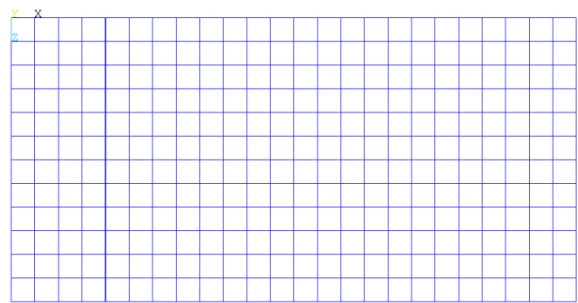


(b)

Fig 5.20 crack pattern plan view in a) unwrapped masonry b) wrapped masonry at 39MPa load level

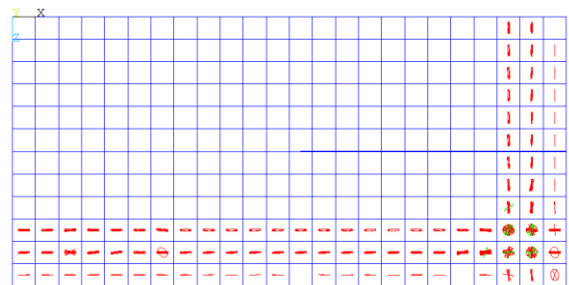


(a)

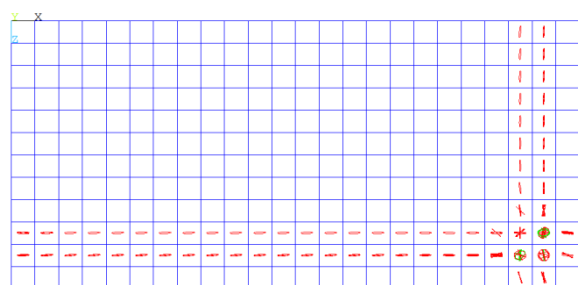


(b)

Fig 5.21 crack pattern plan view in a) unwrapped masonry b) wrapped masonry at 40MPa load level



(a)



(b)

Fig 5.22 crack pattern plan view in a) unwrapped masonry b) wrapped masonry at 40.74MPa load level

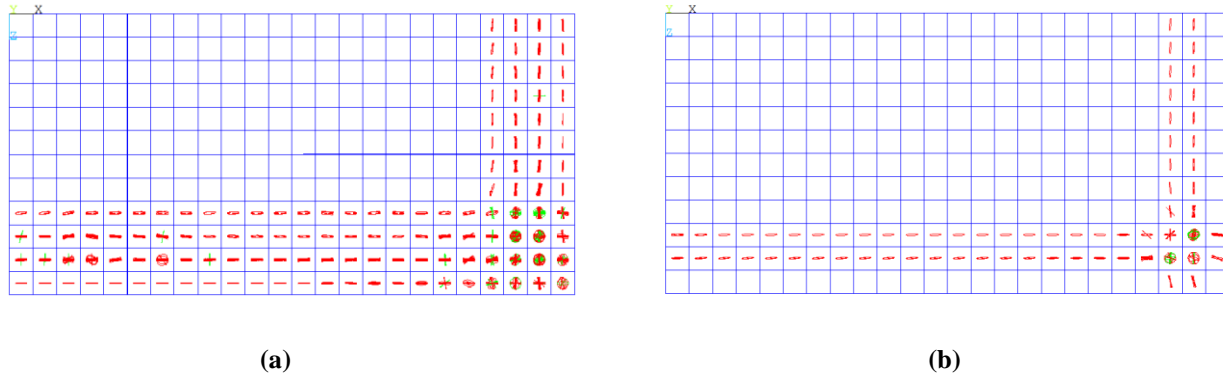


Fig 5.23 crack pattern plan view in a) unwrapped masonry b) wrapped masonry at 41.88MPa load level

5.4 Summary and conclusions

FRCM wrapped brick masonry specimens exhibit increased axial load carrying capacity when compared to that of unwrapped masonry specimens. The final failure resulting from premature failure of the wrapping is relatively more brittle than the failure in unwrapped specimens.

In FRCM wrapped specimens, dilatancy is observed in both brick and mortar. Dilatancy is observed at a stress level which is slightly higher than the unwrapped masonry specimen. The load response from unwrapped and wrapped masonry is similar up to a load level where mortar exhibits significant lateral expansion due to dilatancy. While unwrapped specimen fails after the onset of dilatant behavior in mortar due to increase tensile stress in bricks which produce tensile splitting cracks, wrapped specimen continues to take load because confinement provided by the FRCM which prevents expansion, reducing the level of tensile stress in the brick. Final failure of the wrapped specimens was due to the failure of wrapping in the portion of overlap present in the wrapping. The confinement provided by the FRCM wrapping is effective at the corners for a rectangular specimen, where the masonry bears against the wrapping.

The interaction between the two materials and the internal stress states in brick and mortar are studied using a finite element analysis. Comparison of the load responses of unwrapped and wrapped specimens from the finite element analysis indicated that the role of confinement provided by the FRCM is not effective up to the end of the linear part of load response, where mortar exhibits dilatancy in the unwrapped specimens. There is a decrease in the expansion of the mortar, which reduces the tensile stress in the brick, producing a lower level of damage in the brick at any load level. Analysis indicates that the load carrying capacity can be increased beyond the stress level at failure due to premature rupture of FRCM obtained from experiments.

Chapter 6

Conclusions and recommendations for future work

6.1 Conclusions

The compressive behavior of brick masonry has been investigated and following are the conclusions that can be made from the work presented in this thesis.

When compressive load is applied on stack bonded brick masonry, brick and mortar exhibit linear elastic response until the onset of dilatancy in the confined response of mortar. This dilatant behavior of mortar produces increased tensile stresses in brick which produces cracking in the brick. This behavior leads to vertical splitting of brick at the joint. The vertical crack propagates through the entire column and ultimately produces failure of the specimen.

Fiber reinforced cementitious matrix was used for strengthening of brick masonry. FRCM wrapped specimens showed increased load carrying capacity and failure associated with the premature failure of the wrapping is more brittle. Wrapping is not effective in the initial stages of loading when lateral expansion is small. The confinement provided by FRCM is effective after the onset of dilatancy in mortar. Confinement provided by FRCM increases vertical stiffness of mortar and decreases lateral expansion of mortar, this decreases the tensile forces on brick. Wrapping produces less damage on brick in the form of observed cracking. Brittle failure mode of wrapped specimen can be controlled by preventing failure in wrapping system or by inducing progressive failure in the wrapping system.

6.2 Recommendations for future work

With the use of more advanced and accurate full field strain measurement techniques such as digital image correlation, advancements in this field can give edge for understanding more difficult problems that arise with increase in complexity of the structure. Some fields that are required further research are listed below

- Brittle failure mode of wrapped masonry should be controlled with the use of innovative techniques. Overlap of the wrap needed to be paid more attention.

- Effect of multiple layers of wrapping needs to be investigated
- Study can be extended to other brick layouts
- Study can be extended to other loading conditions such as seismic loading, in-plane and out of plane shear loading on masonry with the use of DIC technique.

Reference

- [1] Mc Nary W.S, Abrams D.P. Mechanics of masonry in compression. J. Struct Eng ASCE 111(4), (1985) 857–870.
- [2] Hemanth. B. kaushik, Durgesh. C. Rai and Sudhir. K. Jain. Stress-strain characteristics of clay brick masonry under uniaxial compression. Current Science, (2007) VOL. 92, NO. 4.
- [3] Vermeltfoort Ad. Brick mortar interaction in masonry under compression. Bouwstenen 85, 2005.
- [4] Uday Vyas Ch. V and Venkatarama Reddy B.V. Prediction of solid block masonry prism compressive strength using FE model. Materials and Structures 43, (2010) 719–735.
- [5] Jahangir Bakhteri, Ahmad Mahir Makhtar and Shamala Sambashivam. Finite element modeling of structural clay brick masonry subjected to axial compression. Journal Teknologi, 41(B), (2004) 57–68.
- [6] Sarangapani. G, Venkatarama Reddy B. V and Jagadish K. S. Structural characteristics of bricks, mortar and masonry. J. Struct. Eng. (India) 29, (2002) 101–107.
- [7] EUROCODE-6. Design of masonry structures. Part 1-1. General rules for buildings: reinforced and unreinforced masonry structures. ENV 1996-1-1, CEN, European Committee for Standardization, Brussels, 1996.
- [8] Korany, Yasser, Glanville, John. Comparing masonry compressive strength in various codes. Concrete international 35, July 2005
- [9] Barbosa C.S, Lourenco P.B, Mohamad G and Hanai J.B. Tri-axial compression tests on bedding mortar samples looking at confinement effect analysis. Tenth North American masonry conference, St Louis, Missouri, USA, 2007.
- [10] Indian Standards (IS), Indian standard code of practice for structural use of unreinforced masonry, IS 1905, 3rd Rev, Bureau of Indian standards, New Delhi, India, 1987.
- [11] Carlo Citto, Shan I. Wo, Kaspar J. Willam and Michael P. Schuller. In-Place evaluation of masonry shear behavior using Digital Image Analysis. ACI materials journal, V.108, No 4, 2011.
- [12] Rashadul Islam Md. Inventory of FRP strengthening methods in masonry structures. Department of construction, Technical university of Catalonia, Barcelona, 2008.
- [13] Marco Di Ludovico, Claudio D’Ambra, Andrea Prota, Gaetano Manfredi. FRP confinement of tuff and clay brick columns: Experimental study and assessment of analytical models. Journal of composites for construction ASCE, Vol. 14, No. 5, (2010) 583 -596.

- [14] Ascione L, Benedetti A, Frassine R, Manfredi G, Monti G, Nanni A, Poggi C and Sacco E. Design Guidelines for the Strengthening of Existing Structures with FRP in Italy. National research council of Italy, execution and control of strengthening interventions by means of fiber reinforced composites. 2004.
- [15] Theofanis D. Krevaikas and Thanasis C. Traintafillou. Masonry confinement with fiber reinforced polymers. Journal of composites for construction ASCE, Vol 9, No.2, (2005) 128-135.
- [16] Antonio Borri, Giulio Castori and Marco Corradi. Masonry columns confined by steel fiber composite wraps. Journal of materials 4, (2011) 311-326.
- [17] Mander J.B, Priestley M.J.N and Park R. Observed stress-strain behavior of confined concrete. Journal of structural engineering ASCE, Vol. 114, No 8, (1988) 1827-1849.